Original Article

MOLECULAR METABOLISM

Partial skeletal muscle-specific Drp1 knockout enhances insulin sensitivity in diet-induced obese mice, but not in lean mice

Benjamin A. Kugler [1], Jared Lourie [1], Nicolas Berger [1], Nana Lin [1], Paul Nguyen [1], Edzana DosSantos [1], Abir Ali [2], Amira Sesay [2], H. Grace Rosen [2], Baby Kalemba [1], Gregory M. Hendricks [3], Joseph A. Houmard [4,5], Hiromi Sesaki [6], Philimon Gona [1], Tongjian You [1], Zhen Yan [7,8], Kai Zou [1,*]

ABSTRACT

Objective: Dynamin-related protein 1 (Drp1) is the key regulator of mitochondrial fission. We and others have reported a strong correlation between enhanced Drp1 activity and impaired skeletal muscle insulin sensitivity. This study aimed to determine whether Drp1 directly regulates skeletal muscle insulin sensitivity and whole-body glucose homeostasis.

Methods: We employed tamoxifen-inducible skeletal muscle-specific heterozygous Drp1 knockout mice (mDrp1$^{+/-}$). Male mDrp1$^{+/-}$ and wildtype (WT) mice were fed with either a high-fat diet (HFD) or low-fat diet (LFD) for four weeks, followed by tamoxifen injections for five consecutive days, and remained on their respective diet for another four weeks. In addition, we used primary human skeletal muscle cells (HSkMC) from lean, insulin-sensitive, and severely obese, insulin-resistant humans and transfected the cells with either a Drp1 shRNA (shDrp1) or scramble shRNA construct. Skeletal muscle and whole-body insulin sensitivity, skeletal muscle insulin signaling, mitochondrial network morphology, respiration, and H_2O_2 production were measured.

Results: Partial deletion of the Drp1 gene in skeletal muscle led to improved whole-body glucose tolerance and insulin sensitivity ($P < 0.05$) in diet-induced obese, insulin-resistant mice but not in lean mice. Analyses of mitochondrial structure and function revealed that the partial deletion of the Drp1 gene restored mitochondrial dynamics, improved mitochondrial morphology, and reduced mitochondrial Complex I- and II-derived H_2O_2 ($P < 0.05$) under the condition of diet-induced obesity. In addition, partial deletion of Drp1 in skeletal muscle resulted in elevated circulating FGF21 ($P < 0.05$) and in a trend towards increase of FGF21 expression in skeletal muscle tissue ($P = 0.095$). In primary myotubes derived from severely obese, insulin-resistant humans, ShRNA-induced-knockdown of Drp1 resulted in enhanced insulin signaling, insulin-stimulated glucose uptake and reduced cellular reactive oxygen species (ROS) content compared to the shScramble-treated myotubes from the same donors ($P < 0.05$).

Conclusion: These data demonstrate that partial loss of skeletal muscle-specific Drp1 expression is sufficient to improve whole-body glucose homeostasis and insulin sensitivity under obese, insulin-resistant conditions, which may be, at least in part, due to reduced mitochondrial H_2O_2 production. In addition, our findings revealed divergent effects of Drp1 on whole-body metabolism under lean healthy or obese insulin-resistant conditions in mice.

Keywords Mitochondrial fission; Mitochondrial dynamics; Insulin sensitivity; Mitochondrial H_2O_2

1. INTRODUCTION

Skeletal muscle insulin resistance is a hallmark characteristic of obesity and has a central role in the development of type 2 diabetes [1]. Extensive efforts have gone into understanding the mechanisms of skeletal muscle insulin resistance to reduce the risk of metabolic diseases. However, the underlying mechanisms of skeletal muscle insulin resistance remain unclear.

Recent research has indicated that mitochondrial dysfunction, including reduced respiration and/or increased ROS generation (e.g., H_2O_2), is linked to the pathogenesis of skeletal muscle insulin resistance [2,3]. Mitochondria are dynamic organelles that undergo cycles of fusion and fission, known as mitochondrial dynamics [4]. Mitochondrial dynamics allow the mitochondria to adapt to their cellular environment and segregate dysfunctional mitochondria to be targeted for autophagic degradation (i.e., mitophagy) to maintain mitochondrial quality and

[1]Department of Exercise and Health Sciences, Robert and Donna Manning College of Nursing and Health Sciences, University of Massachusetts Boston, Boston, MA, USA [2]Department of Biology, University of Massachusetts Boston, Boston, MA, USA [3]Department of Radiology, University of Massachusetts Chan Medical School, Worcester, MA, USA [4]Department of Kinesiology, East Carolina University, Greenville, NC, USA [5]Human Performance Laboratory, East Carolina University, Greenville, NC, USA [6]Department of Cell Biology, Johns Hopkins University, Baltimore, MD, USA [7]Fralin Biomedical Research Institute Center for Exercise Medicine Research, Virginia Tech Carilion, Roanoke, VA, USA [8]Department of Human Nutrition, Foods, and Exercise, College of Agriculture and Life Sciences, Virginia Tech, Blacksburg, VA, USA

*Corresponding author. Department of Exercise and Health Sciences, University of Massachusetts Boston, Boston, MA 02125, USA. E-mail: kai.zou@umb.edu (K. Zou).

Received January 20, 2023 • Revision received August 22, 2023 • Accepted September 5, 2023 • Available online 9 September 2023

https://doi.org/10.1016/j.molmet.2023.101802

Abbreviations

WT	Wild type
mDrp1$^{+/-}$	Skeletal muscle-specific heterozygous tamoxifen-induced Drp1 partial knockout mice
Drp1	Dynamin-related protein 1
MFF	Mitochondrial fission factor
Mid51	Mitochondrial dynamics proteins of 51 kDa
Fis1	Fission protein 1
Mfn1	Mitofusin 1
Mfn2	Mitofusin 2
Opa1	Optic atrophy 1
HFD	High-fat diet
LFD	Low-fat diet
ROS	Reactive oxygen species
mtROS	Mitochondrial reactive oxygen species
H_2O_2	Hydrogen Peroxide
4-HNE	Hydroxynonenal
FGF-21	Fibroblast growth factor 21
HOMA-IR	Homeostatic Model Assessment of Insulin resistance
GTT	Glucose tolerance test
ITT	Insulin tolerance test
AUC	Area under the curve
RCR	Respiratory control ratio

function [5–8]. However, obesity causes the imbalance of mitochondrial dynamics with a shift towards a pro-fission state, leading to fragmented mitochondrial networks in skeletal muscle [9,10]. Dynamin-related protein 1 (Drp1) is a critical regulator of mitochondria fission [11,12]. We and others have shown that Drp1 is hyperactivated in the skeletal muscle from insulin-resistant humans with obesity [9,13,14]. In addition, numerous studies, including ours, have demonstrated a strong inverse correlation between Drp1-mediated mitochondrial fission and skeletal muscle and/or whole-body insulin sensitivity, indicating that Drp1 may serve as a critical regulator of insulin sensitivity [13–16].

In attempts to investigate the direct contribution of Drp1 in regulating skeletal muscle and whole-body insulin sensitivity, many studies have utilized the administration of a Drp1 pharmacological inhibitor (i.e., Mitochondrial Division Inhibitor 1, Mdivi-1). While improvements in insulin action were found in studies when Drp1-mediated mitochondrial fission was inhibited [17–19], a recent study provided evidence suggesting that Mdivi-1 may have off-target effects [20]. Therefore, it remains unclear whether direct reduction of Drp1 is sufficient to improve skeletal muscle and whole-body insulin sensitivity *in vivo* and its underlying mechanism.

To specifically define the causal role of Drp1 in regulating skeletal muscle insulin sensitivity and whole-body glucose homeostasis *in vivo*, we employed a mouse model of skeletal muscle-specific Drp1 heterozygous partial knockout mice (mDrp1$^{+/-}$). Recently, skeletal muscle Drp1 knockout models have been utilized to understand the role of skeletal muscle Drp1 in normal, healthy conditions [21–24]. However, no one has utilized this murine model to study the direct role of skeletal muscle Drp1 in regulating skeletal muscle insulin sensitivity and whole-body glucose metabolism in obese and insulin-resistant conditions, as well as to compare its role under different health conditions. To add a translational perspective, we further examined whether loss of Drp1 in primary human skeletal muscle cells (HSkMCs) derived from humans with severe obesity and insulin resistance could improve skeletal muscle insulin sensitivity. We hypothesized that reducing Drp1 would rebalance mitochondrial dynamics machinery, improve mitochondrial integrity and function, leading to enhanced skeletal muscle and whole-body insulin sensitivity in obesity-induced insulin-resistant conditions, but not in a lean healthy condition.

2. METHODS

2.1. Animal study

2.1.1. Generation of skeletal muscle-specific Drp1 heterozygous mice (mDrp1$^{+/-}$)

Female C57BL/6J mice with flox sites flanking exons 3–5 of the Dnm1L gene (referred to as Drp1$^{fl/fl}$, provided by Dr. Hiromi Sesaki at Johns Hopkins University [25]) were bred with male mice carrying a skeletal muscle-specific tamoxifen-inducible Cre recombinase driven by a human alpha-skeletal actin promoter (HSA-MerCreMer, #031934, The Jackson Laboratory, Bar Habor, ME). This breeding scheme generated tamoxifen-inducible skeletal muscle-specific heterozygous Drp1 knockout mice (mDrp1$^{+/-}$) and littermate wild-type mice (WT) that served as controls. All animals were genotyped based on the presence of HSA-Cre and heterozygous Drp1 flox expression using genomic DNA. All mice were housed based on genotype in a temperature and light-controlled (12:12 h light–dark) room with free access to food and water.

2.1.2. Experimental design

Eight-week-old male WT and mDrp1$^{+/-}$ mice were randomly assigned to either a high-fat diet (HFD, 45% kcal by fat, D12451, Research Diets: New Brunswick, NJ) or a low-fat diet (LFD, 10% kcal by fat, D12450J, Research Diets, New Brunswick, NJ). After four weeks of the diet intervention, mDrp1$^{+/-}$ mice received intraperitoneal injections of tamoxifen (75 μg/g body weight) for 5 consecutive days to induce the skeletal muscle-specific Drp1 knockout. WT mice also received tamoxifen injections as controls to offset the potential effects of tamoxifen. All mice remained on their respective diet for another 4 weeks following the last tamoxifen injection. The diet and muscle-specific Drp1 knockout created four groups: WT/LFD, mDrp1$^{+/-}$/LFD, WT/HFD, and mDrp1$^{+/-}$/HFD (Supplementary Fig. 1A). In addition, a separate set of mice was utilized for the skeletal muscle insulin signaling experiment. Body weight and food consumption were recorded weekly throughout the study. Food consumption (g per week) was converted to kcal (LFD – 3.82 kcal/g, HFD – 4.7 kcal/g) consumed per day (kcal/day). All experimental procedures were approved by the Institutional Animal Care and Use Committee of the University of Massachusetts Boston.

2.1.3. Glucose tolerance and insulin tolerance tests

Intraperitoneal glucose tolerance test (GTT) and insulin tolerance test (ITT) were performed before the tamoxifen injection (to confirm insulin resistance) and 4 weeks after the final tamoxifen injection, as previously described [26]. Briefly, mice were fasted for 6 h and given an intraperitoneal injection of either glucose (1 mg/kg body weight) or insulin (0.75 U/kg body weight). Tail vein blood samples were collected to assess glucose concentrations using a Contour next blood glucometer (Ascensia Diabetes Care, Parsippany–Troy Hills, NJ). The area under the curve (AUC) and inverse AUC was calculated for GTT and ITT, respectively [27,28].

2.1.4. Tissue collection

Animals were fasted overnight (12 h) before tissue collection. Euthanization was performed using CO_2 asphyxiation/cervical dislocation.

Blood was collected and centrifuged for 15 min at 2,500 rpm to collect serum. The gastrocnemius, liver, and heart were then collected, weighed, snap-frozen in liquid nitrogen, and stored at −80 °C for subsequent immunoblot analysis and mitochondrial enzymatic activity. The other gastrocnemius muscle was collected and frozen in pre-cooled isopentane for subsequent immunohistochemistry analysis. Freshly dissected quadriceps were collected for mitochondrial respiration and H_2O_2 production. For insulin signaling data collection, the gastrocnemius muscle tissue was collected 10 min after an intraperitoneal insulin injection (0.75 U/kg body weight).

2.1.5. Transmission electron microscopy

Fresh skeletal muscle tissue was immediately fixed in 2.5% glutaraldehyde in 0.1 M Sodium Cacodylate buffer (pH 7.2) for 24 h at 4 °C and postfixed in 1% osmium for 1 h. Fixed tissues were dehydrated in a series of ascending ethanol concentrations, followed by two propylene oxide baths, and infiltrated using resin SPI-Pon 812 resin mixture per instructions and then switched to Resin/100% Propylene Oxide mixture (1:1), to polymerize overnight at 60 °C. Thin sections (70 nm) of polymerized Epon—Araldite blocks were cut using a Leica Ultracut UCT ultramicrotome placed on Cu grids (200 mesh size), and stained for 5 min in uranyl acetate, followed by 2 min in lead citrate. Muscle fibers were examined on a FEI (ThermoFisher) Tecnai Spirit 12 transmission electron microscope and images captured using a Gatan Rio9, 9-megapixel side-mounted digital camera. Ten representative micrographs from subsarcolemmal and intermyofibrillar regions were acquired at ×25,000 magnification. Quantification was achieved using the Nikon Elements software by manually outlining mitochondria and converting these to actual size using a calibration grid [29].

2.1.6. Immunohistochemistry analysis

To assess skeletal muscle fiber size and fiber type composition, three transverse cryosections of the gastrocnemius muscle (8 μm) were cut using a Leica Cryostat (Leica Biosystems, Buffalo Grove, IL) and placed on microscope slides (Superfrost; Fischer Scientific, Hanover Park, IL). For immunostaining, sections were fixed in 4% formaldehyde for 10 min at 4 °C, followed by permeabilization in 0.25% Triton X-100 for 10 min at 4 °C and then blocked with goat serum (10% in PBS) for 1 h at room temperature. Muscle sections were then incubated for 2 h at room temperature with the following primary antibodies: mouse anti-MCH type I (BA-F8, 1:25, Developmental Studies Hybridoma Bank), mouse anti-MCH type IIa (SC-71, 1:25, Developmental Studies Hybridoma Bank) and anti-MCH IIb (BF-F3, 2:25, Developmental Studies Hybridoma Bank) and rabbit IgG polyclonal anti-laminin (NB300-144, Novus Biological). Muscle sections were then washed 3 times with PBS before being incubated for 1 h with the following secondary antibodies: goat anti-mouse-IgM-FITC (Thermo Fisher Scientific, Waltham, MA), goat anti-mouse IgG-Alexa Fluor 405 (Jackson ImmunoResearch), goat anti-mouse IgG H&L 647 (Jackson ImmunoResearch). These sections were washed in PBS, and coverslips were mounted using Vectashield antifade mounting medium (Vector Laboratories). Slides were imaged using a Zeiss confocal microscopy (Carl Zeiss AG) at ×10 magnification. To analyze muscle fiber size and type, analyses were performed using MyoVision software following the instructions [30].

2.1.7. Serum insulin and FGF21

Serum was collected during the tissue collection process. Following the manufacturer's protocol, fasting serum insulin and FGF21 concentrations were measured using an Insulin (EMINS, Thermo Fisher Scientific, Waltham, MA) or FGF21 (RayBiotech, Peachtree Corners, GA) ELISA Kit.

2.1.8. Skeletal muscle mitochondria isolation

Skeletal muscle mitochondria were isolated as previously described [18]. Briefly, the quadriceps muscle was dissected and placed in an ice-cold isolation buffer for mitochondria 1 (IBM1, 67 mM sucrose, 50 mM Tris—HCl, 50 mM KCl, 10 mM EDTA, and 0.2% BSA, pH 7.4). The skeletal muscle was minced on ice, placed in IBM1 with 0.1% trypsin solution for 30 min, and then centrifuged at 200 *g* for 3 min. The pellet was then resuspended in IBM1, homogenized on ice using a glass Teflon homogenizer, and centrifuged at 800 *g* for 10 min. The supernatant was collected and centrifuged at 8,000 *g* for 10 min to pellet the mitochondria. The pellet was then washed and resuspended in an ice-cold isolation buffer for mitochondria 2 (IBM2, 250 mM sucrose, 2 mM EGTA, and 10 mM Tris—HCl, pH 7.4) and centrifuged at 8,000 *g* for 10 min. The pelleted mitochondria were resuspended in cold IBM2, and protein concentration was determined using a Pierce BCA protein assay kit (Thermo Fisher Scientific, Waltham, MA). All steps were performed at 4 °C.

2.1.9. Skeletal muscle mitochondrial respiration

Seahorse XFp Analyzer (Agilent Technologies, Santa Clara, CA) was used to determine mitochondrial respiratory rates by measuring oxygen consumption rates (OCR) in isolated mitochondria as previously described [18]. Briefly, isolated mitochondria were plated on a seahorse XFp extracellular flux analyzer plate at a 4 μg/well concentration. Pre-warmed pyruvate (10 mM) + malate (5 mM) or palmitoyl-L-carnitine (40 μM) + malate (1 mM) solution was added to each well. The following substrates were successively injected to measure OCR for different respiration rates: pyruvate + malate or palmitoyl-L-carnitine + malate to measure state 2 respiration rate, ADP (5 mM) to measure state 3 respiration rate, oligomycin (2 μM) to measure state 4 respiration rate, carbonyl cyanide-4 phenylhydrazone (FCCP, 4 μM) to measure maximal respiration rate, and antimycin (4 μM) to measure non-mitochondrial respiration rates. Respiratory exchange ratio (RCR) was calculated by state 3 respiration rate ÷ state 4 respiration rate and used to assess mitochondrial integrity. All data were analyzed using the Agilent Seahorse Wave software.

Additionally, the seahorse XFp Analyzer (Agilent Technologies, Santa Clara, CA) determined HSkMCs cellular respiratory rates by measuring the OCR as previously described [14,18]. On the day of the assay, media was changed to XF Assay Medium containing modified DMEM (no phenol red and glucose) supplemented with 5 mM glucose and 2 mM glutamine and placed in a non-CO_2 37 °C incubator for 30 min prior to the start of the assay. Oligomycin (1 μM), FCCP (0.75 μM), and rotenone/antimycin A (0.5 μM) were successively injected to measure OCR for different respiratory states. OCR coupled to ATP production was calculated by basal OCR (measurement before oligomycin injection) − lowest OCR measurement following oligomycin injection. All data were normalized to protein concentrations for each well.

2.1.10. Skeletal muscle mitochondrial-derived H_2O_2 production

Mitochondrial-derived H_2O_2 production (JH_2O_2) was measured fluorometrically as previously described [31]. Briefly, JH_2O_2 was measured in Buffer Z (105 mM K-MES, 30 mM KCl, 1 mM EGTA, 10 mM K_2HPO4, 5 mM $MgCl_2$-$6H_2O$, 2.5 mg/mL BSA, pH 7.1), supplemented with creatine (5 mM), creatine kinase (20 U/mL), phosphocreatine (30 mM, to mimic resting condition), amplex ultra red (10 μM), horseradish peroxidase (20 U/mL), superoxide dismutase (20 U/mL), ATP (5 mM), and auranofin (0.1 μM). The following substrates assessed various sites: (1) pyruvate (5 mM) + malate (2.5 mM) to assess Complex I via generation of NADH; (2) pyruvate (5 mM) + malate (2.5 mM) + antimycin (2 mM) for the assessment of Complex III; (3)

succinate (10 mM) + rotenone (4 mM) to assess Complex II via generation of FADH [32], and (4) palmitoyl-L-carnitine (40 mM) + malate (1 mM) to assess H_2O_2 production during fatty acid oxidation. All reactions were done at 37 °C, 200 μL of volume, and 15 μg of mitochondria in a microplate reader (Thermo Fisher Scientific, Waltham, MA). Fluorescence values were converted to picomoles of H_2O_2 via an H_2O_2 standard curve, and H_2O_2 emission rates were calculated as picomoles of H_2O_2 per minute per milligram [33].

2.1.11. Mitochondrial enzyme activity

The activity of citrate synthase and Complex I and II enzymes were analyzed using the Citrate Synthase Assay kit (ab239712, Abcam, Waltham, MA) Complex I Enzyme Activity Assay Kit (ab109721, Abcam, Waltham, MA) and Complex II Enzyme Activity Microplate Assay Kit (ab109908, Abcam, Waltham, MA) according to the manufacturer's instructions. Briefly, gastrocnemius was homogenized in cold phosphate-buffered saline (PBS), and the protein concentration was measured using a Pierce BCA Protein Assay Kit (Thermo Fisher Scientific, Waltham, MA). Samples were loaded into the wells at a concentration of 40μg/100 μL (Citrate Synthase), 250 μg/200 μL (Complex I), and 60μg/50 μL (Complex II).

2.2. Human skeletal muscle cell (HSkMC) culture model

2.2.1. Primary human skeletal muscle cell culture

Previously isolated HSkMCs from severely obese, insulin-resistant, and lean insulin-sensitive humans were used in this study [14,18,34]. In brief, HSkMCs were thawed (n = 6 per group), pooled together, and grown in growth media as previously described [18]. At a confluence of ~80%, myoblasts were subcultured onto a 6-well type I collagen plate (Corning, Glendale, AZ), 35 mm collagen-coated glass-bottom dish (MatTek, Ashland, MA), Seahorse XFp cell culture miniplate (Agilent Technologies, Santa Clara, CA), or 96 well transparent bottom black polystyrene microplate (Corning, Glendale, AZ) depending on experimental purposes. Upon reaching ~80% confluency, myoblasts were switched to low-serum (2% horse serum) media to induce differentiation. All experiments were performed on day 7 of differentiation. The experimental protocol was approved by the Internal Review Board for Human Research at the University of Massachusetts Boston.

2.2.2. Lentivirus-mediated Drp1 knockdown

Plasmid encoding shRNA for human Drp1 (shDrp1, Cat #TRCN0000318426) was obtained from Sigma Aldrich (Natick, MA). Packaging vectors psPAX2 (Cat #12260), envelop vector pMD.G (Cat #12259), and shRNA scramble (shScramble, Cat #1864) were obtained from Addgene (Watertown, MA). 293T cells in a 10 cm dish were transfected using polyethyleneimine hydrochloride (Polysciences, Inc, Warrington, PA) with 2.66 μg of psPAX2, 0.75 μg pMD2.G, and 3 μg of shRNA plasmid. After 48 h, the media was collected, filtered using a 0.45 μm vacuum filter, and used to treat undifferentiated myoblast on experimental plates. After 48 h, target cells were selected with puromycin to confirm knockdown success. Growth media was switched to differentiation media at a ~80–90% confluence (Supplementary Fig. 1B).

2.2.3. Quantification of mitochondrial network morphology

The mitochondrial morphology was quantified as previously described [14]. Briefly, myotubes were stained with MitoTracker™ RedFM (100 nM, Thermo Fisher Scientific, Waltham, MA) for 15 min. Zeiss confocal microscopy was then used to image the myotubes mitochondrial network using a 64 × 1.4NA oil objective. Fifteen images per repeat were taken for quantification. Images were analyzed using the mitochondrial network analysis macro (MiNA) tool developed on FIJI distribution of ImageJ as previously described [35]. For image analysis, images were preprocessed via an unsharp mask with a two-pixel radius, enhancement of local contrast (CLAHE), filtered to remove background, binarized, and skeletonized for further analysis. Individual non-networked mitochondria, the number of mitochondrial networks, branch length per network, and the number of branches per network were quantified using a previously developed protocol [35]. Data from each image was normalized by total mitotracker intensity per nucleus.

2.2.4. Quantification of glucose uptake

Differentiated myotubes were serum-starved in serum-free DMEM for 3 h. Myotubes were treated with or without 100 nmol/L of insulin for 1 h. Glucose uptake assay was then performed using an assay kit provided by Cayman Chemical (Ann Arbor, MI), following the manufacturer's protocol.

2.2.5. Reactive oxygen species

Myotubes grown on 96-well plates were washed in prewarmed PBS, incubated with 1 μM CM-H2DCFDA (Thermo Fisher Scientific, Waltham, MA) in non-phenol red DMEM at 37 °C for 30 min with 5% CO_2, and washed again with PBS. Fluorescence was measured by a microplate reader (Thermo Fisher Scientific, Waltham, MA) with an excitation wavelength of 490 nm and an emission wavelength of 520 nm. Data were normalized to the protein concentration for each well.

2.3. Immunoblotting

Tissues and cell lysates were homogenized as previously described [18]. Protein concentrations from the cell lysates, gastrocnemius, liver, and heart, were determined by a Pierce BCA Protein Assay Kit (Thermo Fisher Scientific, Waltham, MA), and equal amounts of protein were subjected to SDS-Page using a 4–20% gradient polyacrylamide gel (Bio-Rad, Hercules, CA) and transferred to a nitrocellulose membrane. Membranes were probed with a primary antibody and rocked overnight at 4 °C. Membranes were then probed with an IRDye secondary antibody (Li-COR, Lincoln, NE) and quantified using the Odyssey CLx software (Li-Cor, Lincoln, NE). All data were normalized to GAPDH protein expression. A complete list of all suppliers, catalog numbers, and dilutions for primary and secondary antibodies used in this study are found in Supplementary Table 1. Skeletal muscle insulin action was determined by the fold change of basal over insulin-stimulated phosphorylation of Akt Ser^{473}, calculated by dividing the insulin-stimulated phosphorylation of Akt Ser^{473} protein expression by the average non-insulin stimulated phosphorylated Akt Ser^{473} protein expression.

2.4. Statistical analyses

For each group, data was summarized using mean ± SEM. The interaction over time between group and body weight, GTT, and ITT were analyzed using repeated-measures analysis of variance (rANOVA). In addition, comparisons between groups were performed by two-way ANOVA effect of genotype (WT vs. $mDrp1^{+/-}$) and diet (LFD vs. HFD), followed by Fisher's LSD post-hoc analysis when significant interactions were detected. Pearson correlation analysis was used to assess linear relationships. One-way ANOVA was used to compare the differences between groups in the HSkMC model, followed by Fisher's LSD post-hoc analysis where indicated. All statistical analyses were performed using SPSS statistical software (27.0; SPSS, Inc, Chicago, IL). Statistical significance was set at $P < 0.05$.

3. RESULTS

3.1. Partial Drp1 knockout in skeletal muscle does not affect food consumption, body weight, or skeletal muscle weight

We first confirmed that HFD-induced obesity as HFD-fed mice had higher body and epididymal fat pad weights (7.66% and 152.1%, respectively) than LFD-fed mice (main effect of diet, $P < 0.05$, Table 1). However, no differences were found in the heart and skeletal muscle tissue weights. Overall, there was no genotype effect on calorie consumption, body weight, or tissue weight (Table 1).

3.2. Partial Drp1 knockout in skeletal muscle altered mitochondrial dynamics towards pro-fusion state and mitochondrial morphology without any changes in mitochondrial biogenesis, fusion, or mitophagy protein markers

The partial reduction of Drp1 protein expression was confirmed in the gastrocnemius muscle from mDrp1$^{+/-}$ mice (Figure 1A). There was a significant reduction in Drp1 protein expression in gastrocnemius muscle from mDrp1$^{+/-}$ mice compared to the WT group (~32%, main effect of genotype, $P < 0.05$, Figure 1A). Additionally, there was a main effect of diet on Drp1 protein expression in the gastrocnemius muscle, with HFD-fed mice having a greater Drp1 expression than LFD-fed mice (~17% $P < 0.05$, Figure 1A). There were no differences in Drp1 protein expression in other tissues among groups (Figure 1A). Taken together, these data confirmed the successful partial Drp1 knockout in skeletal muscle only.

We next assessed the impact of the partial Drp1 knockout on proteins that regulate mitochondrial dynamics. Phosphorylation of Drp1(Ser^{616}), a marker of Drp1 activity, was significantly downregulated in skeletal muscles from the partial Drp1 knockout mice, regardless of diet (main effect of genotype, $P < 0.05$, Figure 1B). The ratio of pDrp1(Ser^{616}) over total Drp1 was also significantly decreased in skeletal muscles from the partial Drp1 knockout mice fed with HFD ($P < 0.05$), but not LFD (Figure 1B). Furthermore, the protein content of mitochondrial fission factor (MFF), a mitochondrial fission adapter protein, was greater in mDrp1$^{+/-}$ mice when compared to WT mice (main effect of genotype, $P < 0.05$, Figure 1B). There was no diet or genotype effect in the protein expression of any other markers of mitochondrial fission or fusion. (Figure 1B and C). To further assess the balance between mitochondrial fission and fusion, we generated ratios of pDrp1(Ser^{616}) over the three fusion protein markers (i.e., Mfn1, Mfn2 and Opa1). Partial Drp1 knockout significantly reduced the ratios of pDrp1(Ser^{616})/Mfn2 and pDrp1(Ser^{616})/Opa1, regardless of diet (main effect of genotype, $P < 0.05$, Figure 1D). In addition, Partial Drp1 knockout significantly reduced the ratios of pDrp1(Ser^{616})/Mfn1in mice fed with HFD ($P < 0.05$), but not LFD (Figure 1D). Finally, given the important role of mitochondrial dynamics in maintaining mitochondrial morphology, further analysis of mitochondrial structure and morphology was performed using transmission electron microscopy. Skeletal muscle from mDrp1$^{+/-}$ mice fed with HFD exhibited larger mitochondria with a more fused structure in both intermyofibrillar (IMF) and subsarcolemmal (SS) regions when compared to WT mice fed with HFD ($P < 0.05$, Figure 1E and F).

We next assessed markers of other mitochondrial quality control processes and quantity. The partial Drp1 knockout did not alter PGC-1α protein content, despite its content being greater in HFD-fed mice than in LFD-fed mice regardless of genotype (main effect of diet, $P < 0.05$, Figure 2A). There was no diet or genotype effect in the protein expression of any markers of mitophagy/autophagy (Figure 2B). There was no statistically significant main effect of diet or genotype in protein expression of several mitochondrial content markers, including citrate synthase, VDAC, and mitochondrial oxidative phosphorylation Complex I-V (Figure 2C–D). Interestingly, a diet and mDrp1$^{+/-}$ interaction revealed that citrate synthase activity was higher in the mDrp1$^{+/-}$/LFD group than in the WT/LFD and mDrp1$^{+/-}$/HFD groups ($P < 0.05$, Figure 2E). There was no substantial difference in citrate synthase activity between WT/LFD, WT/HFD, and mDrp1$^{+/-}$/HFD groups (Figure 2E).

3.3. Partial Drp1 knockout in skeletal muscle improves whole-body glucose homeostasis and insulin sensitivity in diet-induced insulin-resistant mice

Metabolic tests (GTT and ITT) were first performed before the induction of skeletal muscle Drp1 knockout to confirm an insulin-resistant phenotype in HFD-fed mice (main effect of diet, $P < 0.05$, Supplementary Figs. 2A–D). To determine if the partial loss of skeletal muscle Drp1 is sufficient to alleviate glucose intolerance and insulin resistance, metabolic tests were then performed four weeks after the induction of the partial skeletal muscle Drp1 knockout. Blood glucose levels at all time points during the GTT test and the AUC of blood glucose were significantly elevated in HFD-fed mice compared to LFD-fed mice (main effect of diet, $P < 0.05$, Figure 3A and B). Interestingly,

Table 1 — Animal characteristics.

	WT-LFD	mDrp1$^{+/-}$LFD	WT-HFD	mDrp1$^{+/-}$HFD
Food Consumption (kcal per day)	12.44 ± 0.45	12.55 ± 0.36	13.76 ± 0.37*	13.70 ± 0.38*
Body Weight				
Starting (g)	24.1 ± 0.25	24.1 ± 0.42	23.5 ± 0.30	23.9 ± 0.36
Final (g)	28.1 ± 0.25	28.0 ± 0.44	30.3 ± 0.65*	30.2 ± 0.67*
Percent Bodyweight gained (%)	16.8 ± 1.0	16.8 ± 1.6	29.3 ± 2.4*	26.6 ± 2.5*
Tissue Weight (g/g of body weight)	0.154 ± 0.004	0.152 ± 0.004	0.153 ± 0.003	0.151 ± 0.003
Gastrocnemius				
Tibialis Anterior	0.049 ± 0.003	0.050 ± 0.003	0.055 ± 0.004	0.050 ± 0.003
Heart	0.145 ± 0.004	0.138 ± 0.004	0.137 ± 0.007	0.140 ± 0.008
Epididymal fat pad	0.469 ± 0.032	0.436 ± 0.035	1.186 ± 0.123*	1.10 ± 0.134*
Fasting Glucose (mg/dL)	162.0 ± 6.39	168.9 ± 5.0	191.2 ± 7.2*	190.6 ± 6.7*
Fasting Insulin (μIU/ml)	22.0 ± 3.17	22.4 ± 10.72	40.6 ± 4.51	26.7 ± 8.21
HOMA-IR	8.93 ± 1.20	9.89 ± 4.77	20.45 ± 2.46*	12.33 ± 3.76*

Note: Data are presented as mean ± SEM. $n = 5–16$/group.
AbbreviationHOMA-IR, Homeostatic Model Assessment of Insulin Resistance (fasting insulin concentration [μIU/mL] x fasting glucose concentration [mg/dl]/405).
*$p < 0.05$ diet effect.

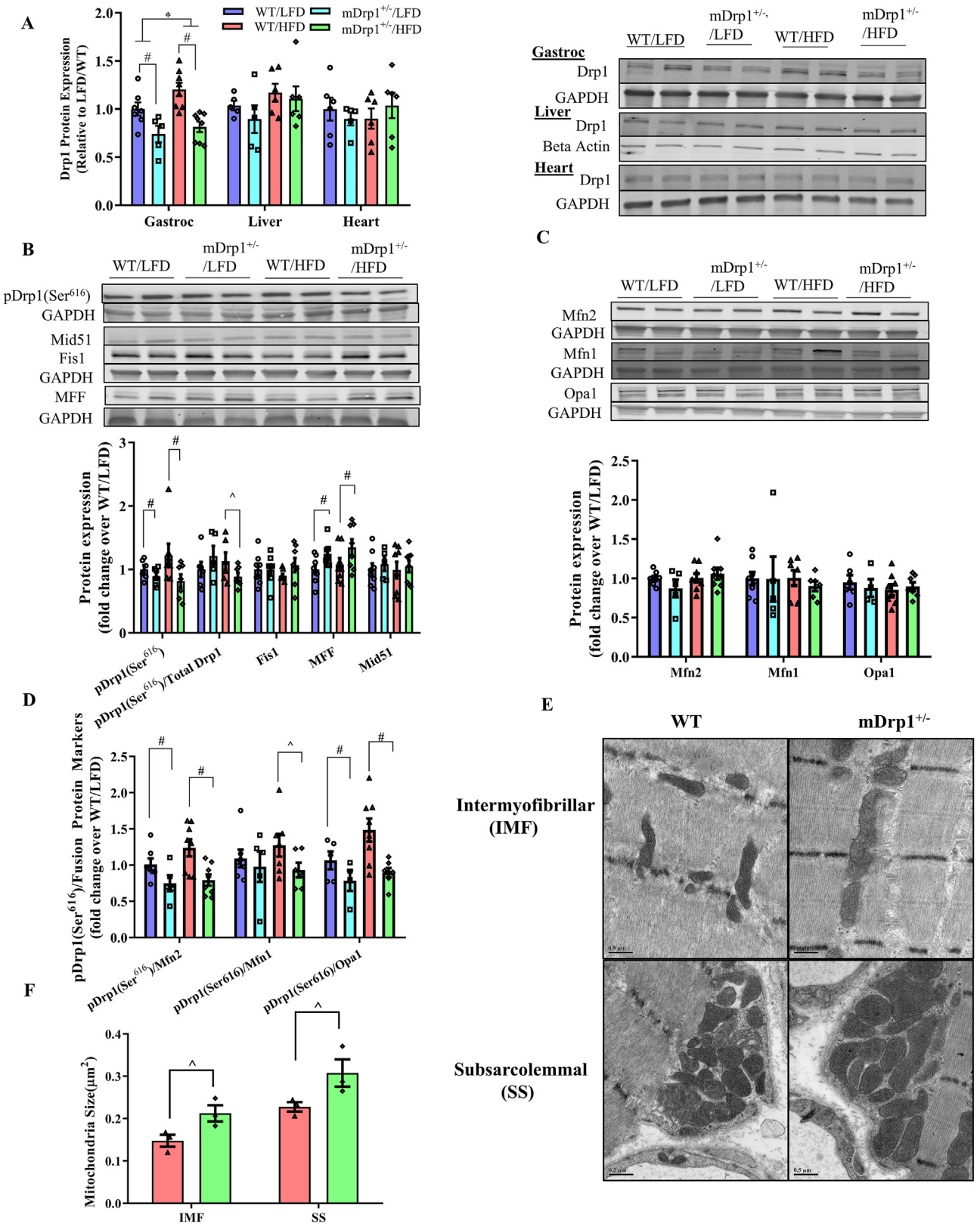

Figure 1: Validation of partial knockout of skeletal muscle Drp1, protein expression of mitochondrial dynamics markers and mitochondrial morphology in skeletal muscle from WT and mDrp1$^{+/-}$ mice fed either a LFD or HFD. (A) Protein expression and representative immunoblots of Drp1 in gastrocnemius (Gastroc), liver, and heart. (B) Expression of proteins markers of mitochondrial fission and representative immunoblots. (C) Expression of proteins markers of mitochondrial fusion and representative immunoblots. (D) Ratios of pDrp1(Ser616) over mitochondrial fusion protein markers. (E) Representative transmission electron micrographs obtained from intramyofibrillar and subsarcolemmal regions of skeletal muscle. Scale bar = 0.5 μm (F) Quantification of mitochondria size. scale bar = 0.5 μm. Data are presented as mean ± SEM. n = 3–8/group. *p < 0.05 main effect of diet, #p < 0.05 main effect of genotype. ^p < 0.05 vs. indicated group.

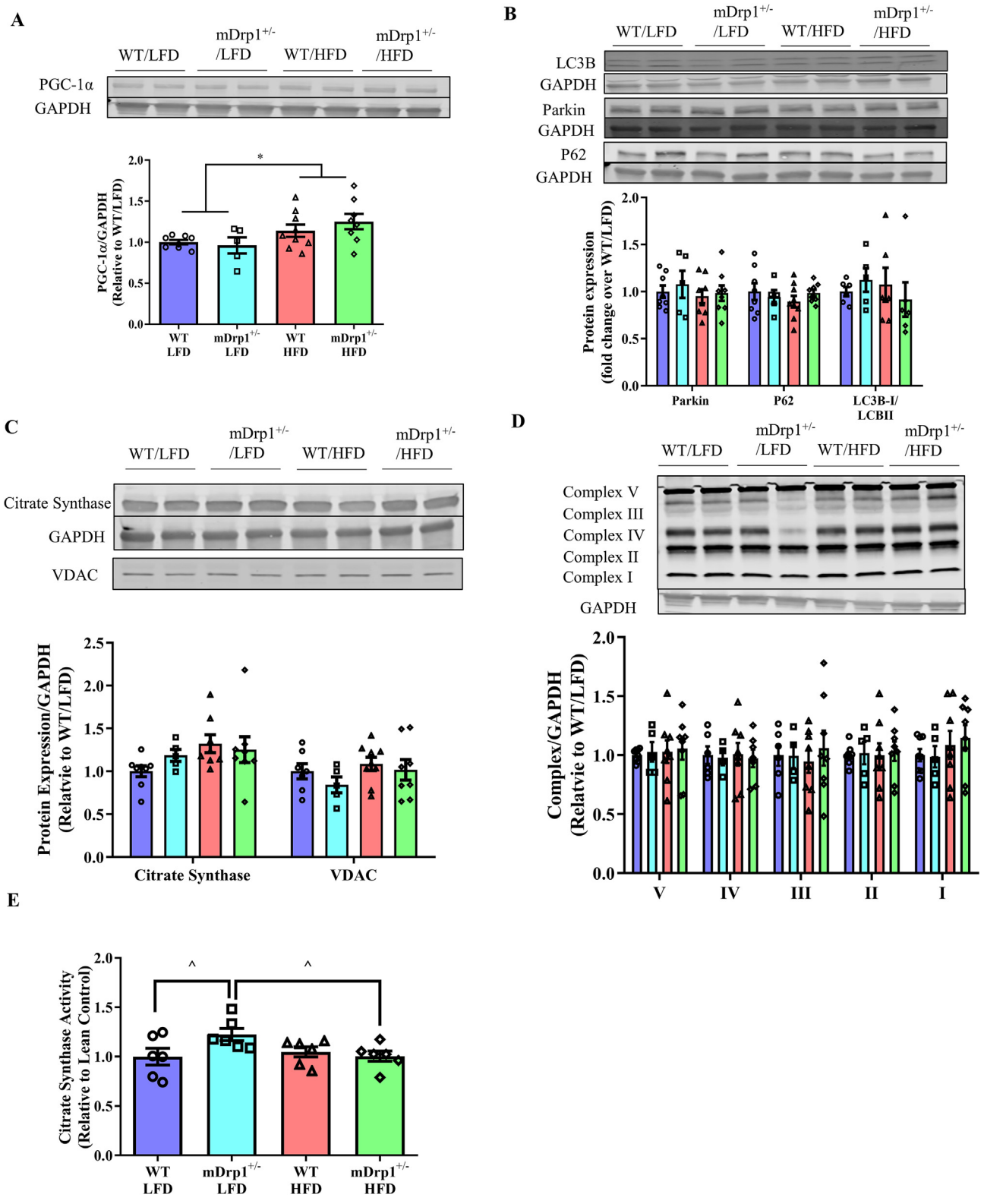

Figure 2: Protein expression of mitochondrial biogenesis, mitophagy/autophagy and content markers in skeletal muscle from WT and mDrp1$^{+/-}$ mice fed either a LFD or HFD. (A) PGC-1α protein expression and representative immunoblot. (B) Expression of protein markers of mitophagy/autophagy and representative immunoblots. (C) Protein expression of mitochondrial content makers (Citrate Synthase and VDAC) and representative immunoblots. (D) OXPHOS protein content and representative immunoblot. (C) Citrate synthase activity. Data are presented as mean ± SEM. n = 5–8/group. *p < 0.05 main effect of diet, ^p < 0.05 vs. indicated group.

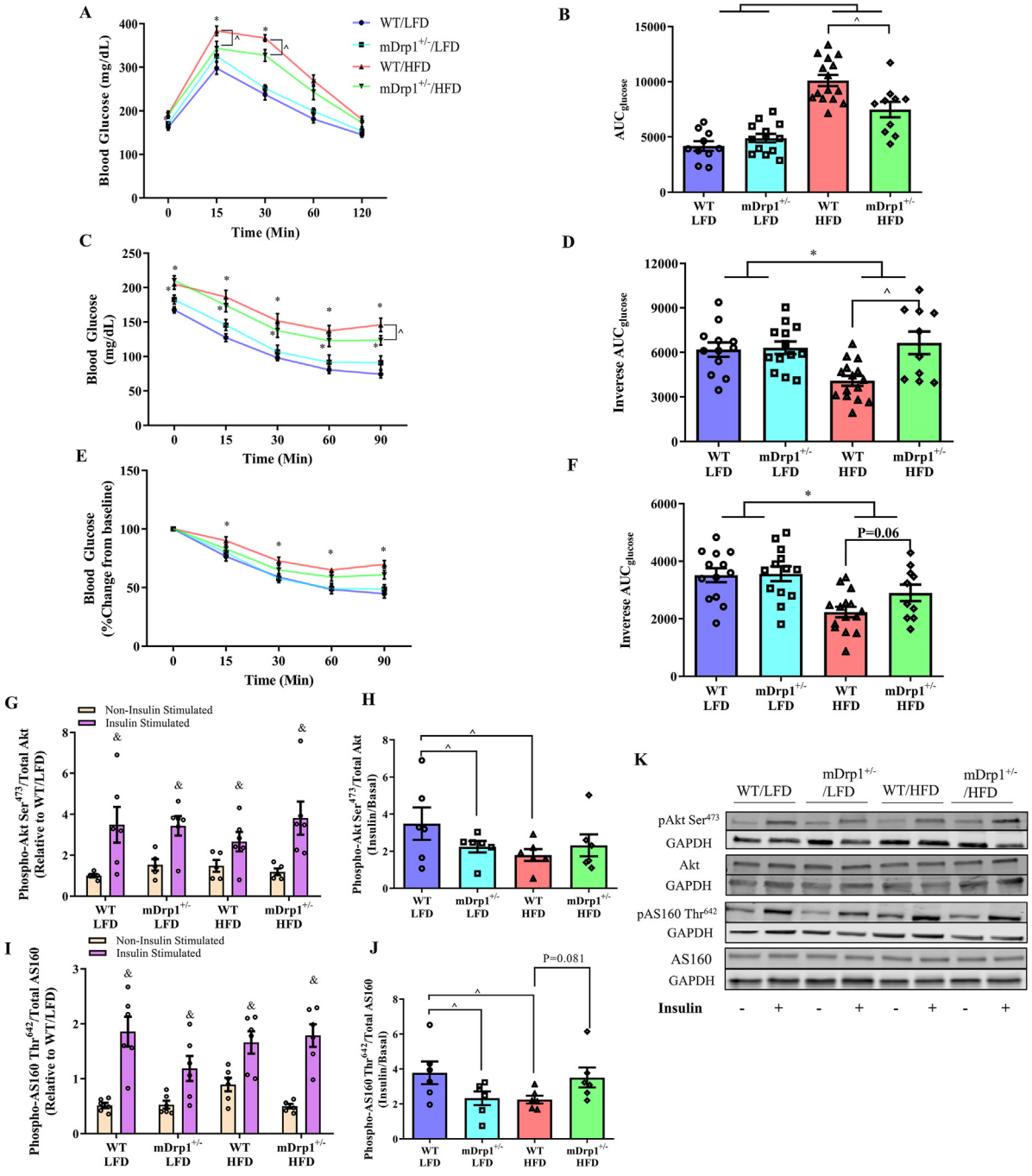

Figure 3: Whole-body insulin sensitivity and skeletal muscle insulin signaling in WT and mDrp1$^{+/-}$ mice fed either a LFD or HFD. (A) Blood glucose levels during GTT. (B) Blood glucose area under the curve (AUC) during GTT. (C) Blood glucose levels during ITT. (D) Inverse glucose area under the curve (AUC) during ITT. (E) Relative blood glucose levels (percent change from baseline) during ITT. (F) Inverse glucose area under the curve (AUC) during ITT based on relative blood glucose levels. (G) Phosphorylation of Akt Ser^{473}/Akt under non-insulin stimulated and insulin stimulated conditions. (H) Fold change in Akt Ser^{473} phosphorylation/Akt under insulin stimulated over non-insulin stimulated conditions. (I) Phosphorylation of AS160 Thr^{642}/AS160 under non-insulin stimulated and insulin stimulated conditions. (J) Fold change in AS160 Thr^{642}/AS160 under insulin stimulated over non-insulin stimulated conditions. (K) Representative Blots of (G) and (I). Data are presented as mean ± SEM. $n = 6–13$/group. *p < 0.05 main effect of diet, #p < 0.05 main effect of genotype, ^p < 0.05 vs indicated group, & p < 0.05 vs. respective non-insulin stimulated condition.

a significant diet and genotype interaction was found during the GTT, revealing that at 15 and 30 min, there is a reduction in blood glucose levels in mDrp1$^{+/-}$/HFD compared to WT/HFD mice ($P < 0.05$, Figure 3A). In addition, there was a moderate but significant reduction in AUC of blood glucose in GTT (35.2%) in mDrp1$^{+/-}$/HFD mice compared to WT/HFD mice ($P < 0.05$, Figure 3B). Similarly, Blood glucose levels at all time points during the ITT test were higher in HFD-fed mice in comparison to LFD-fed mice (Figure 3C). Importantly, blood glucose level at 90-minute timepoint during ITT test was significantly lower in mDrp1$^{+/-}$/HFD mice compared to WT/HFD mice ($P < 0.05$, Figure 3C). In addition, there was a greater inverse AUC of blood glucose in ITT, whether expressed in absolute or relative values, in

mDrp1$^{+/-}$/HFD mice when compared to the WT/HFD mice ($P = 0.01$ and $P = 0.06$, respectively. Figure 3D and F). Finally, fasting blood glucose levels and HOMA-IR were elevated in HFD-fed mice (15.1% and 75.2%, respectively) (main effect of diet, $P < 0.05$, Table 1). Although not statistically significant, blood insulin level (P = 0.11) and HOMA-IR (P = 0.10) value were reduced by 32.3% and 39.9%, respectively, in mDrp1$^{+/-}$/HFD mice compared to the WT/HFD mice (Table 1). There was no difference in GTT, ITT, fasting glucose, insulin, and HOMA-IR values between WT/LFD and mDrp1$^{+/-}$/LFD mice.

To assess skeletal muscle insulin signaling, the phosphorylation of Akt Ser^{473} and AS160 Thr^{642} was measured. Upon insulin stimulation, the phosphorylation of Akt Ser^{473} and AS160 Thr^{642} were elevated in skeletal muscles from mice in all groups (main effect of insulin, $P < 0.05$, Figure 3G and I). There were no significant differences in insulin-stimulated phosphorylation of these two molecules between any two groups (Figure 3G and I). To further assess their responses to insulin stimulation, fold change (ratio of insulin-stimulated over basal values) was calculated. A diet and genotype interaction was noted in the fold change of both Akt Ser^{473} and AS160 Thr^{642} phosphorylation in response to insulin stimulation, revealing a significant reduction in skeletal muscle from HFD-fed WT mice compared to LFD-fed counterparts ($P < 0.05$, Figure 3H and J). However, while there were modest increase of the fold change of insulin-stimulated Akt Ser^{473} and AS160 Thr^{642} phosphorylation over basal (29.2% and 56.0%, P = 0.163 and 0.081, respectively) in skeletal muscles from mDrp1$^{+/-}$/HFD mice than WT/HFD mice, mDrp1$^{+/-}$/HFD mice did not display any significant improvement in skeletal muscle insulin signaling (Figure 3H and J). Interestingly, partial Drp1 knockout induced significant reductions of the fold change in Akt Ser^{473} and AS160 Thr^{642} phosphorylation in skeletal muscle from LFD-fed mice (mDrp1$^{+/-}$/LFD) when compared to WT/LFD mice (−33.0% and 38.6%, $P < 0.05$, Figure 3H and J). There was no difference in total GLUT 4 content among all groups (Supplementary Fig. 3A).

3.4. Partial Drp1 knockout in skeletal muscle reduces mitochondrial H_2O_2 production in diet-induced insulin-resistant mice

We next sought to determine if the partial Drp1 knockout in skeletal muscle improved mitochondrial function (mitochondrial respiration and H_2O_2 production), which may lead to reduced insulin resistance. There was no difference in mitochondrial respiration with either pyruvate + malate (indicator of glucose oxidation) or palmitoyl-L-carnitine + malate (indicator of fatty acid oxidation) substrates under different respiration states (Figure 4A–D).

Regarding mitochondrial H_2O_2 production, HFD-fed mice overall had a significantly high Complex I- and Complex II-supported H_2O_2 emission in isolated mitochondria compared to LFD-fed mice (main effect of diet, $P < 0.05$, Figure 4E–G). Interestingly, a diet and genotype interaction was found, revealing a reduction in Complex I-supported H_2O_2 emission in mDrp1$^{+/-}$/HFD mice compared to WT/HFD mice ($P < 0.05$, Figure 4E). In addition, mitochondria from mDrp1$^{+/-}$ mice displayed reduced Complex II-supported H_2O_2 emission compared to WT mice (main effect of genotype, $P < 0.05$, Figure 4F), which appears to be mainly driven by the reduction in mDrp1$^{+/-}$/HFD mice. There was no substantial difference among groups in H_2O_2 emission with pyruvate + malate + antimycin (Complex III-driven, Figure 4H). Finally, there was a trend toward a significant increase in Complex II activity found in mDrp1$^{+/-}$ mice compared to the WT counterparts (main effect of genotype, P = 0.098, Figure 4J). No differences were found in Complex I activity among any groups (Figure 4I). There was no difference in 4-HNE level between any two groups (Figure 4K).

3.5. Partial Drp1 knockout in skeletal muscle does not alter skeletal muscle mass, fiber size, or fiber type distribution

Since previous studies reported that Drp1 knockout in skeletal muscle induced muscle atrophy, we investigated the effect of partial Drp1 knockout on skeletal muscle phenotype. There were no differences in either gastrocnemius or tibialis anterior (TA) muscle mass (Table 1) among the groups. Skeletal muscle fiber size and fiber type distribution were performed on the gastrocnemius (Supplementary Fig. 4A). The gastrocnemius displayed no significant difference in overall myofiber cross-sectional area or each individual fiber type cross-sectional area among groups (Supplementary Figs. 4B–D). In addition, there were no significant differences in fiber type distribution (Supplementary Fig. 4E).

3.6. Partial Drp1 knockout in skeletal muscle increased both skeletal muscle and serum FGF21 level

Since previous studies have reported that alterations in mitochondrial dynamics led to increased circulating FGF21 and FGF21 in linked to whole-body glucose homeostasis and metabolism, we measured FGF21 content in both skeletal muscle tissue homogenates and serum. There were significant elevations of FGF21 protein expression and circulating concentration in muscle tissue homogenates and serum from mDrp1$^{+/-}$ mice, respectively, in comparison to WT mice (main effect of genotype, $P < 0.05$, Supplementary Figs. 5A and B).

3.7. The loss of Drp1 reduced mitochondrial fission and restored the mitochondrial network structure in primary myotubes derived from humans with severe obesity and insulin resistance

To assess the translational application of reducing Drp1 in skeletal muscle to improve insulin sensitivity, we applied the knockdown of Drp1 in HSkMC derived from skeletal muscle biopsy samples of humans with severe obesity and insulin resistance. Participant characteristics are presented in Table 2. Humans with severe obesity exhibited an insulin-resistant phenotype with elevated fasting insulin levels and HOMA-IR compared to lean controls (Table 2, $P < 0.05$).

The transfection of shDrp1 in myotubes derived from humans with severe obesity and insulin resistance resulted in reductions in total Drp1 protein expression and Drp1 phosphorylation (Ser^{616}) (~78% and 51%, respectively) compared to the myotubes derived from shScramble-treated myotubes from the same subjects (Figure 5A, $P < 0.05$). There were no statistically significant differences in the expression of any other mitochondrial fission and fusion protein markers among groups (Figure 5A–C).

We next investigated whether Drp1 knockdown altered mitochondrial network morphology towards a more-fused state. Myotubes derived from humans with severe obesity exhibited a more fragmented mitochondrial network with an increase in the number of non-networked individual mitochondria and mitochondrial networks and a reduction in mitochondrial network size (branch length per network) compared to the lean counterparts (Figure 5F–H, $P < 0.05$). Importantly, the loss of Drp1 restored the mitochondrial network structure with a significant reduction in the number of non-networked individual mitochondria and an increase in branch length per network compared to shScramble-treated myotubes derived from the same donors (Figure 5F and H, $P < 0.05$). There were no group differences in mitochondrial density (P = 0.115) and the number of branches per network (Figure 5E and I).

3.8. The loss of Drp1 enhanced insulin action in primary myotubes derived from humans with severe obesity and insulin resistance

The phosphorylation of Akt Ser^{473} and AS160 Thr^{642} and glucose uptake were all significantly elevated in response to insulin stimulation

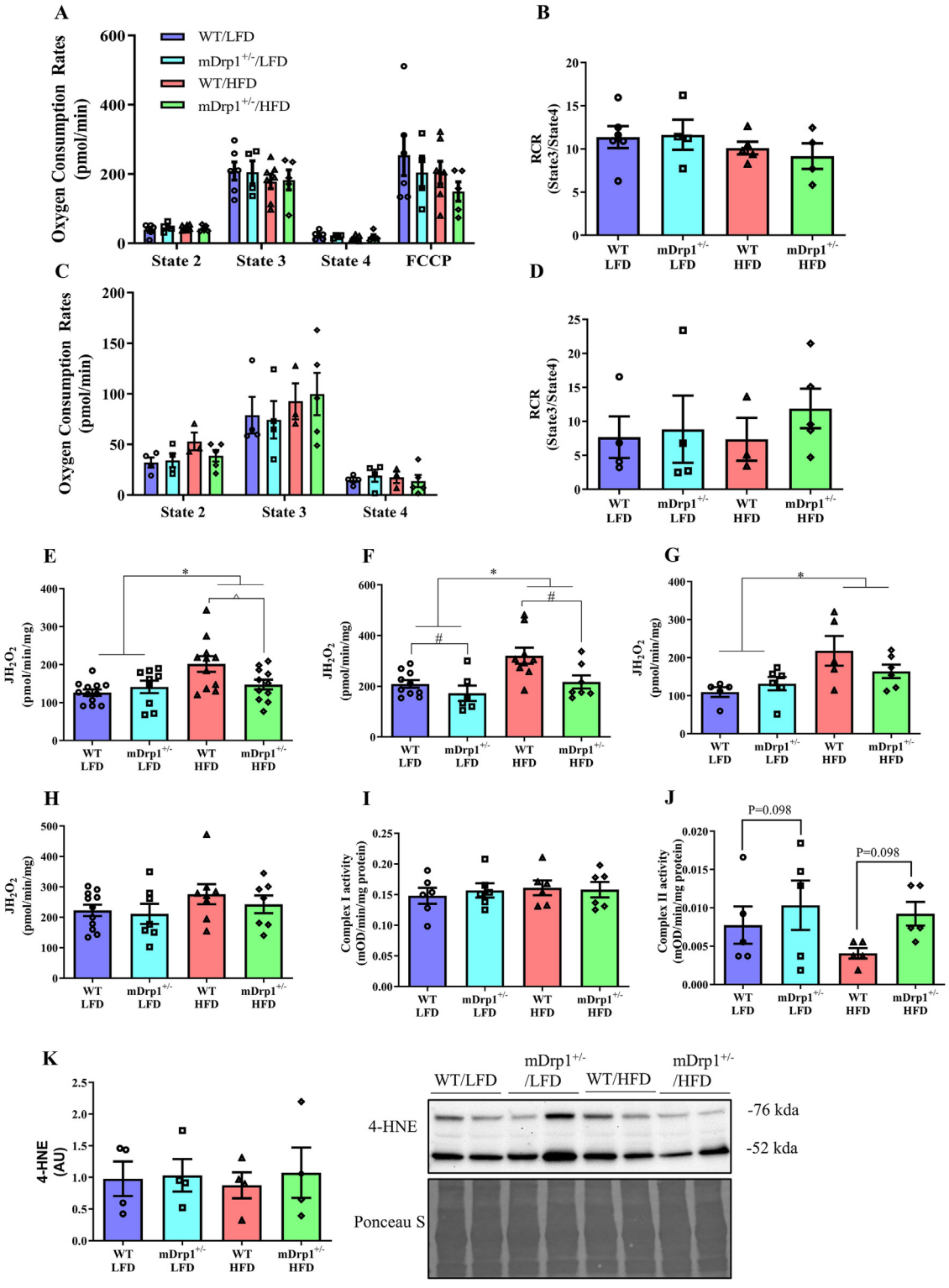

Figure 4: Mitochondrial function in skeletal muscle from WT and mDrp1$^{+/-}$ mice fed either a LFD or HFD. (A) Mitochondrial oxygen consumption rates under different respiration states energized by pyruvate + malate. (B) Respiratory control ratio (RCR, State 3/State 4) energized by pyruvate + malate. (C) Mitochondrial oxygen consumption rates under different respiration states energized by palmitoyl-L-carnitine + malate. (D) Respiratory control ratio (RCR, State 3/State 4) energized by palmitoyl-L-carnitine + malate. (E) Mitochondrial-derived H_2O_2 production rate under pyruvate + malate. (F) Mitochondrial-derived H_2O_2 production rate under succinate + rotenone. (G) Mitochondrial-derived H_2O_2 production rate under palmitoyl-L-carnitine + malate. (H) Mitochondrial-derived H_2O_2 production rate under pyruvate + malate + antimycin. (I) Complex I activity. (J) Complex II activity. (K) 4-HNE content and representative blot. Data are presented as mean ± SEM. n = 3–10/group. *p < 0.05 diet effect, #p < 0.05 mDrp1$^{+/-}$ effect, ^p < 0.05 vs indicated group.

Table 2 — Human subject characteristics.

	Lean	Severely Obese
Race	6C/0AA	4C/2AA
Age	28.8 ± 4.1	39.2 ± 2.5
Weight (kg)	62.3 ± 3.3	145.1 ± 5.6*
BMI (kg/m^2)	23.1 ± 1.6	52.2 ± 2.3*
Fasting glucose (mg/dl)	86.0 ± 2.2	94.6 ± 1.6
Fasting insulin (μIU/ml)	6.7 ± 0.96	17.6 ± 1.79*
HOMA-IR	1.44 ± 0.23	4.11 ± 0.43*

Note: Data are presented as mean ± SEM. $n = 6$ per group.
C Caucasian, *AA* African American, *BMI* body mass index.
Abbreviations: BMI, Body mass index; HOMA-IR, Homeostatic Model Assessment of Insulin (fasting insulin concentration [μIU/ml] x fasting glucose concentration [mg/dl]/405).
*$p < 0.05$ versus Lean.

in all groups (Figure 6A ,C, and F, $P < 0.05$). However, the magnitudes of insulin-induced increases were significantly blunted in myotubes from humans with severe obesity and insulin resistance compared to their lean and insulin-sensitive counterparts (both were treated with Shscramble RNA) (Figure 6A, C and F), and these differences reached significance in AS160 Thr^{642} and glucose uptake ($P < 0.05$). Notably, these significantly reduced responses to insulin stimulation were restored in myotubes from humans with severe obesity and insulin resistance when treated with shDrp1 (Figure 6C and F), $P < 0.05$). Similarly, the ratio of insulin-stimulated phosphorylation of Akt Ser^{473} and AS160 Thr^{642} over basal, and glucose uptake over the basal state, surrogate markers of insulin action, were all significantly enhanced in shDrp1-treated myotubes derived from humans with severe obesity and insulin resistance when compared to the shScramble RNA treated counterparts (Figure 6B, D and G, $P < 0.05$), with virtually no differences compared to the lean and insulin-sensitive controls. No differences were found in total GLUT 4 content between groups (Supplementary Fig. 3B).

3.9. The loss of Drp1 did not alter mitochondrial respiration but reduced reactive oxygen species in myotubes derived from humans with severe obesity and insulin resistance

We next investigated whether the improvement in skeletal muscle insulin sensitivity in myotubes derived from humans with severe obesity and insulin resistance was due to enhanced mitochondrial function. Basal, FCCP-induced maximal, and spare capacity were all significantly lower in myotubes from humans with severe obesity and insulin resistance (Figure 6H, $P < 0.05$). Further, the OCR coupled to ATP production was significantly lower in myotubes from humans with severe obesity and insulin resistance (Figure 6H, $P < 0.05$). While basal and FCCP-induced maximal respiratory rates were increased in shDrp1-treated myotubes compared to the shScramble treated controls (58.9%, Figure 6H), they did not reach statistical significance. They were not fully restored to the levels seen in myotubes derived from lean insulin-sensitive humans. Interestingly, myotubes from humans with severe obesity and insulin resistance had a higher content of cellular ROS than the lean and insulin-sensitive controls (Figure 6I, $P < 0.05$), which was substantially reduced with the loss of Drp1 (Figure 6I, $P < 0.05$). No substantial group differences in mitochondrial content were detected as measured by citrate synthase protein expression (Figure 6J).

4. DISCUSSION

It has been consistently shown that reduced skeletal muscle Drp1-mediated mitochondrial fission coincides with improved skeletal muscle and whole-body insulin sensitivity under insulin-resistant conditions such as obesity [6,14,16–18]. However, the direct role of skeletal muscle Drp1-mediated mitochondrial fission in regulating skeletal muscle insulin sensitivity, and whole-body glucose homeostasis and insulin sensitivity remains untested. Herein, we demonstrated that the reduction in Drp1 via partial knockout of skeletal muscle Drp1 was sufficient to enhance whole-body glucose homeostasis and insulin sensitivity, but not skeletal muscle insulin signaling, in diet-induced insulin-resistant mice. In addition, we demonstrated that these metabolic improvements were, at least partly, due to reduced skeletal muscle mitochondrial H_2O_2 production, resulting from rebalanced mitochondrial dynamics and improved mitochondrial structure.

It is noteworthy that the mDrp1$^{+/-}$ mice fed with HFD exhibited moderate but significant improvements in whole-body insulin sensitivity. Previous studies using genetic approaches to knockdown Drp1 in skeletal muscle to different extents (~34% vs. ~30%) have presented different phenotypes in skeletal muscle physiology [21,24], suggesting Drp1-mediated mitochondrial fission might be sensitive to even subtle modulation and exert different effects on skeletal muscle and whole-body alterations. To extend the findings from the current study, future work should investigate the effects of various degrees of skeletal muscle Drp1 reduction on skeletal muscle and whole-body insulin sensitivity. It should also be noted that our study ended 4 weeks after the induction of the partial loss of Drp1. The mDrp1$^{+/-}$ mice may exhibit more profound improvements in whole-body insulin sensitivity at a later stage following a partial loss of Drp1.

In the present study, while significant improvement of insulin sensitivity was found in human primary myotubes from severely obese humans transfected with shDrp1 *in vitro*, skeletal muscle from partial Drp1 knockout (mDrp1$^{+/-}$/HFD) mice did not display significant improvement of insulin sensitivity in HFD-fed mice. This is against our hypothesis. The divergent results of skeletal muscle and whole-body insulin sensitivity in partial Drp1 knockout mice fed with HFD *in vivo* suggests that partial Drp1 knockout in skeletal muscle may exert effects beyond skeletal muscle tissue and on other metabolic tissues that are responsible for insulin-stimulated glucose uptake (e.g., liver and adipose tissue). One possible explanation is that partial Drp1 knockout in skeletal muscle may alter myokine secretion in skeletal muscle, which are known to affect systemic glucose metabolism and crosstalk with other tissues/organs [36]. One potential regulator is fibroblast growth factor 21 (FGF21), which has been found to improve whole-body glucose metabolism and insulin sensitivity [37,38]. It was recently reported that the ablation of skeletal muscle Drp1 triggered the secretion of muscle-derived FGF21, resulting in improved whole body glucose homeostasis [22]. Indeed, our findings of elevated FGF21 in the partial Drp1 knockout mice are consistent with the literature and support the idea that moderately increased circulating FGF21 in mDrp1$^{+/-}$ mice may contribute to the improved whole-body glucose tolerance and insulin sensitivity despite no enhancement in skeletal muscle insulin sensitivity. Furthermore, the elevated circulating FGF21 can target other metabolic tissues, which may also be responsible for the alleviated insulin resistance at the whole-body level in mDrp1$^{+/-}$/HFD mice. Due to the lack of these tissues collection in the present study, we cannot pinpoint a specific tissue that is responsible for the improvement in whole-body metabolic adaptations in mDrp1$^{+/-}$/HFD mice, which is a limitation of the study. Future studies should be warranted to investigate metabolic adaptations in these tissues to identify the precise mechanisms underlying the alleviation of diet-induced insulin resistance in Drp1 knockout animals. In addition, as a limitation, it is worth noting that we did not measure GLUT4

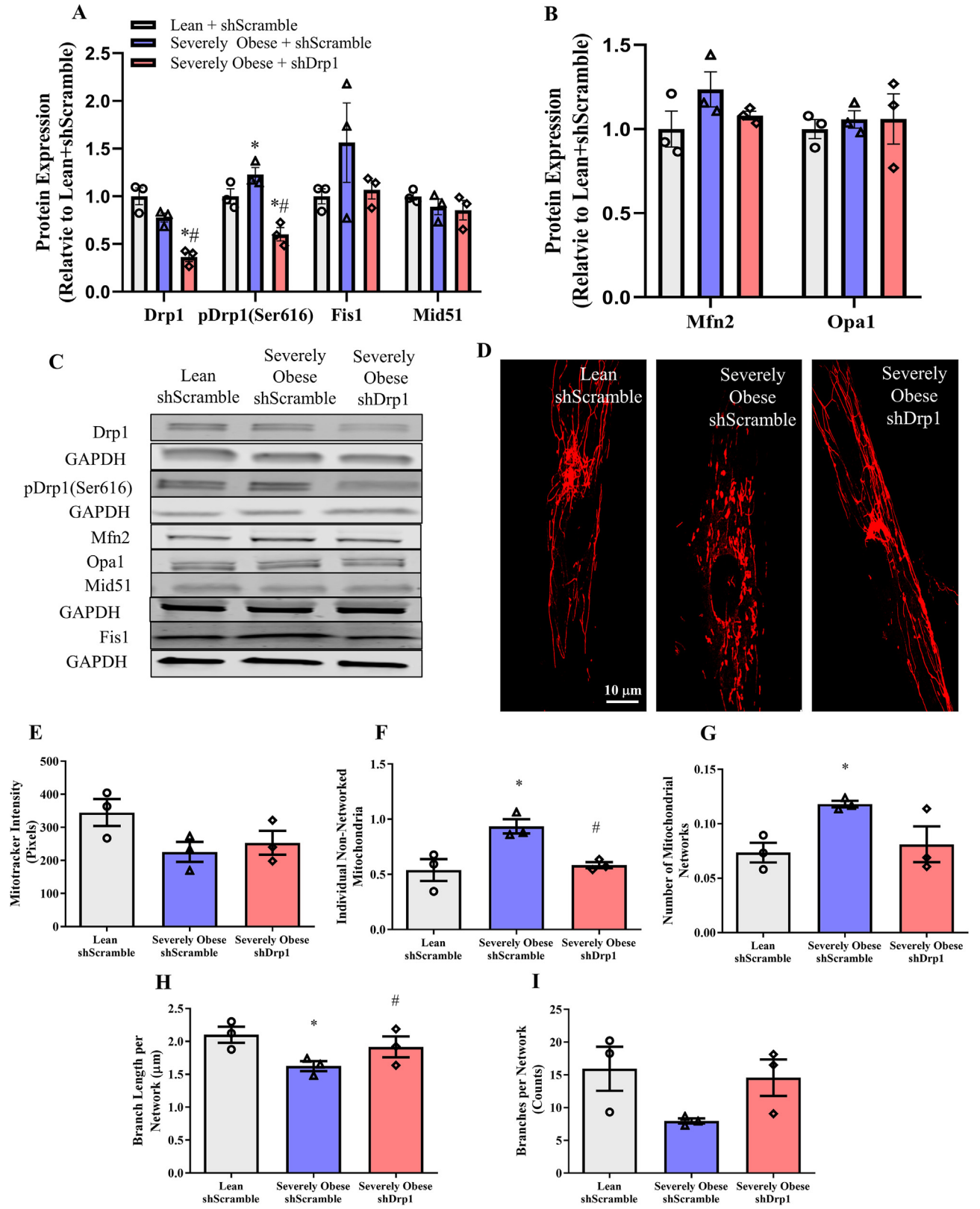

Figure 5: Validation of Drp1 knockdown and protein expression of protein markers of mitochondrial dynamics in primary human myotubes derived from lean, insulin-sensitive with shScramble, and severely obese, insulin-resistant humans with either shScramble or shDrp1. (A) Expression of protein markers of mitochondrial fission. (B) Expression of proteins markers of mitochondrial fusion. (C) Representative immunoblots for (A) and (B). (D) Representative images of myotubes stained with MitoTracker RedFM. Scale bar = 10 µm. (E) Mitotracker intensity. (F) Number of individual non-networked mitochondria. (G) Number of mitochondrial networks. (H) Average branch length per network (network size). (I) Number of branches per network (network size). Data are presented as mean ± SEM. n = 3 independent experiments of HSkMCs pooled samples from six lean, insulin-sensitive, and six severely obese, insulin-resistant humans. *p < 0.05 versus Lean shScramble; #p < 0.05 versus Severely Obese shScramble.

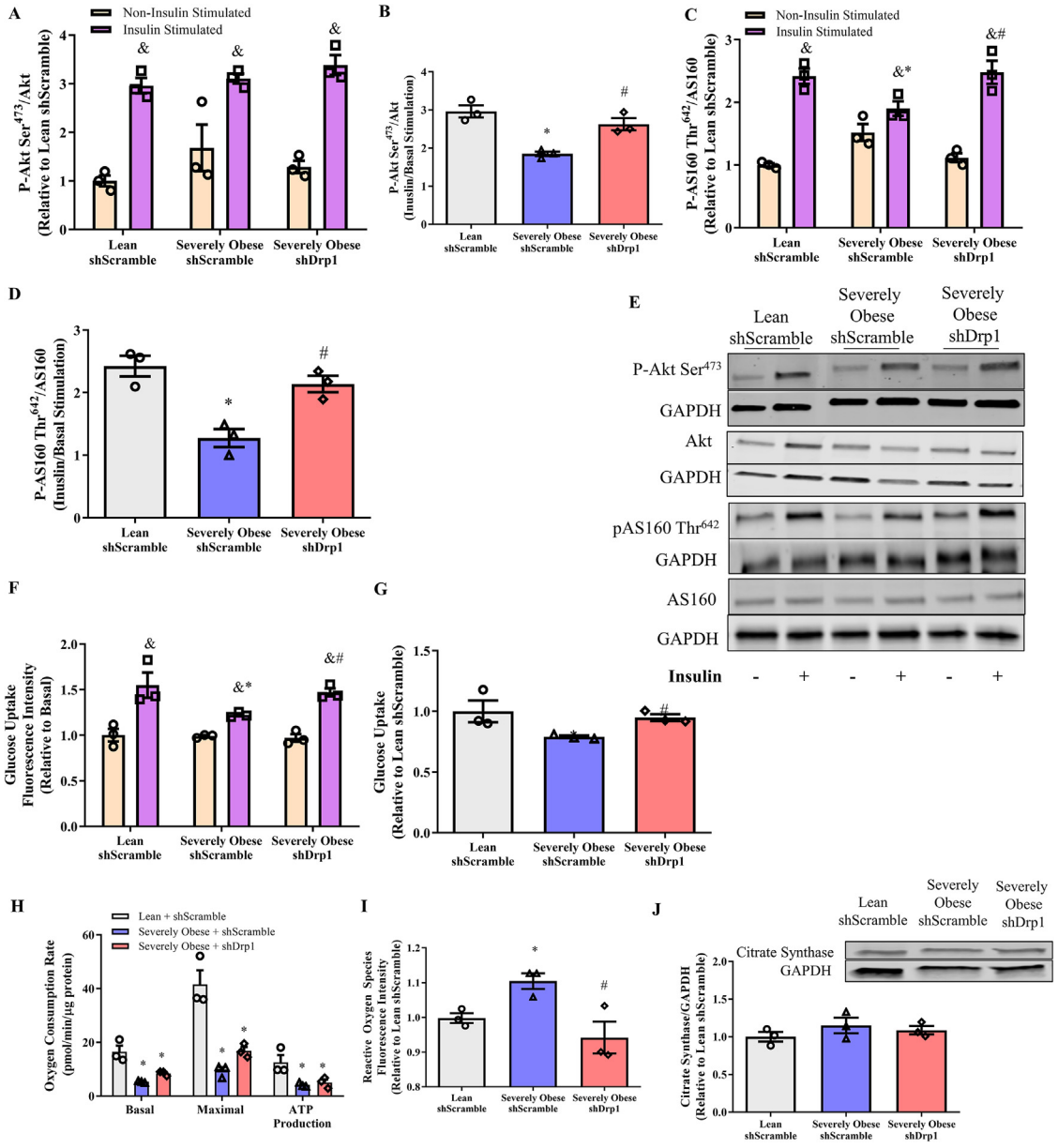

Figure 6: Insulin action and mitochondrial function in myotubes derived from lean, insulin-sensitive with shScramble, and severely obese, insulin-resistant humans with either shScramble or shDrp1. (A) Akt Ser^{473} phosphorylation/Akt under non-inuslin and insulin stimulated conditions. (B) Fold change in Akt Ser^{473} phosphorylation/Akt under insulin stimulated conditions over non-insulin stimulated conditions. (C) Phosphorylation of AS160 Thr^{642}/AS160 non-insulin and insulin stimulated conditions. (D) Fold change in AS160 Thr^{642}/AS160 under insulin stimulated conditions over non-insulin stimulated conditions (E) Representative blots for (A) to(D). (F) Glucose uptake under non-insulin stimulated, and insulin stimulated conditions. (G) Fold change in glucose uptake under insulin stimulated condition over non-insulin stimulated condition. (H) Oxygen Consumption Rate (OCR); (I) Intracellular reactive oxygen species (ROS) levels. (J) Citrate synthase protein expression and representative blot. Data are presented as mean ± SEM. $n = 3$ independent experiments of HSkMCs pooled samples from six lean, insulin-sensitive, and six severely obese, insulin-resistant humans. *p < 0.05 versus Lean shScramble; #p < 0.05 versus Severely Obese shScramble; & p < 0.05 versus respective non-insulin stimulated condition.

translocation or ex vivo insulin-stimulated glucose uptake using skeletal muscle tissue. Therefore, we cannot completely rule out the role of Drp1 in directly regulating skeletal muscle insulin sensitivity.

Mitochondrial dynamics is a complex system, with multiple mechanisms that can regulate mitochondrial quality and whole-body metabolism. Previous studies have reported smaller mitochondria, an indication of a fragmented mitochondrial network, with a reduction in Mfn2 protein in skeletal muscle from both obese rodents and humans [39,40]. Further, the reduction of Mfn2 gene expression was associated with suppressed glucose disposal rates [39]. Nonetheless, we and others have reported no changes in mitochondria fusion proteins but an increase in mitochondrial fission in short-term feeding of a HFD [17,18,41], suggesting that there are acute and chronic adaptations of mitochondrial dynamics involved in the development of insulin resistance. Similarly, it has been reported that the knockout of skeletal muscle Drp1 induces an increase in Opa1 content [22,24], which was not observed in the current study. However, the degree of skeletal muscle Drp1 loss may influence mitochondrial fusion markers, as a previous study utilizing the same partial skeletal muscle Drp1 knockout model observed no differences in mitochondrial fusion proteins [21].

However, unexpectedly, the present study did find a greater protein expression of the mitochondrial fission adaptor protein MFF in mDrp1$^{+/-}$ mice (Figure 1C). MFF is vital for the initial recruitment of Drp1 to the outer mitochondrial membrane [42,43]. Therefore, the increase in MFF in mDrp1$^{+/-}$ mice may be an attempt by the mitochondria to counteract the reduction in Drp1 via a compensatory mechanism to initiate mitochondrial fission. Current knowledge regarding MFF's function beyond mitochondrial fission is scarce. Future investigations on whether MFF plays a role and/or serves as a downstream molecule of Drp1 in regulating skeletal muscle insulin sensitivity are warranted. Lastly, in regard to mitochondrial content, there were no significant changes in mitochondrial content in skeletal muscle from HFD-fed mice or primary myotubes derived from severely obese and insulin resistant humans as indicated by several protein markers. These results are consistent with several previous studies with the similar duration of HFD intervention or human muscle cell culture model [44–48], but conflict with a couple studies where either longer period of HFD intervention was applied or myotubes from T2D humans were studied [44,49]. Taken together, it suggests that mitochondrial content does not change until later in the development of insulin resistance and T2D.

In the present study, several markers of mitochondrial health were improved in skeletal muscle from mDrp1$^{+/-}$ mice fed with HFD, including rebalanced mitochondrial dynamics, improved mitochondrial integrity, and reduced mitochondrial ROS production (mtROS). Mitochondria are a significant source of ROS production in skeletal muscle, as superoxide that leaks from the mitochondria is converted to H_2O_2 [50]. Our findings corroborated with several previous studies reporting inhibiting Drp1 activity enhanced mitochondrial dynamics and network architecture and mitigated the increase in overall mitochondrial-driven ROS content [17–19,51], but further extend these findings by demonstrating that such mitigation is likely due to a reduction in mitochondrial H_2O_2 production. Interestingly, we did not observe any reduction of 4-HNE (a product of lipid peroxidation), a marker of cellular ROS content. This would suggest that the mitigation of insulin resistance in partial Drp1KO mice was not due to the mitigation of overall ROS level, but rather due to mitochondrial H_2O_2 production. Anderson et al. reported that attenuating mitochondrial H_2O_2 production was sufficient to improve whole-body insulin sensitivity in an animal model of diet-induced insulin resistance [52]. Taken together, our findings align with previous studies and suggest that the partial loss of Drp1 in skeletal muscle under insulin resistant condition leads to rebalanced mitochondrial dynamics, improved mitochondrial integrity, and reduced mitochondrial H_2O_2 production, resulting in enhanced whole-body metabolic improvements.

Numerous sites involved in mtROS production have been identified (e.g., Complexes I, II, and III) [32,53,54]. Our results suggest two significant sites for mtROS production (Complex I and II). Complex I and III are traditionally thought to be significant sites of mtROS. In the current study, the partial knockout reduced Complex I mtROS production in mice fed a HFD, however, there were no differences in Complex I activity. There are several non-respiratory chain sites of superoxide/H_2O_2 production, including the matrix dehydrogenase enzyme pyruvate dehydrogenase, which are active when testing Complex I mtROS [55], suggesting non-respiratory chain sights may be influencing complex I mtROS production. Nonetheless, a recent study reported that Complex II generates mtROS at significantly high rates [32]. Herein, we demonstrate that Complex II-supported mtROS production was reduced, likely due to the enhanced Complex II activity in our partial Drp1 knockout mouse model fed with HFD. Interestingly, reduced Complex II activity in peripheral tissues induced by obesity has been associated with impaired insulin sensitivity [56–58]. Further, enhanced skeletal muscle Complex II activity has been previously shown after utilizing an insulin sensitizer [59]. Taken together, these data suggest that improved Complex II activity and associated suppression in mtROS production may be responsible for improved skeletal muscle insulin sensitivity in mDrp1$^{+/-}$ mice. Interestingly, reducing Drp1 content does not alter Complex II-supported mtROS production in our LFD-fed healthy mice. This is consistent with a previous study conducted by Dulac and colleagues [24], which further corroborates the notion that reducing Drp1 in skeletal muscle may exert divergent effects on skeletal muscle physiology in healthy and insulin-resistant conditions.

Although the Drp1 knockdown significantly affected mtROS production in human myotubes derived from severely obese humans, there were no significant changes in mitochondrial respiration. We speculate that 1) there may be impairments in other sites of metabolic pathways before entering the electron transport chain system (e.g., TCA cycle, glucose transporter) so that there was a compromised availability of substrate for mitochondria myotubes derived from severely obese humans to oxidize; 2) there may be an intrinsic impairment in mitochondrial respiratory capacity (e.g., genetic factors) in muscle cells derived from severely obese humans in comparison to normal lean humans. Regardless, our results from human myotubes suggest that impaired mitochondrial respiration may not be a cause of skeletal muscle insulin resistance. Various studies have failed to observe a correlation between mitochondrial respiration and skeletal muscle insulin resistance as there were no reduction in skeletal muscle mitochondrial respiration rates until skeletal muscle insulin resistance was established [60,61]. In addition, the overfeeding of non-obese sedentary individuals induces insulin resistance without altering markers of mitochondrial content or mitochondrial oxidative capacity, suggesting insulin resistance arises independently from reduced mitochondria respiration [62]. Therefore, Drp1 may not regulate mitochondrial respiration, but regulates mitochondrial H_2O_2 emission, which has been associated with regulating insulin sensitivity.

Mitochondria act as hubs for cellular signaling by actively mediating the flux of secondary messengers such as calcium (Ca^{2+}). Previous studies have reported that mitochondrial depolarization is accompanied by a rise in cytosolic Ca^{2+} activating calcineurin, which in turn activates Drp1. Interestingly, the loss of calcineurin in skeletal muscle, results in hyperfused mitochondria via reduction of Drp1 activity, which preserved glucose tolerance and insulin sensitivity in mice fed a HFD [63], indicating Ca^{2+} signaling regulates insulin sensitivity through Drp1. However, the loss of skeletal muscle Drp1-mediated mitochondrial fission has been reported to alter Ca^{2+} handling, as the ablation of skeletal muscle Drp1 induces an increase in mitochondrial Ca^{2+} uptake, reducing cytosolic Ca^{2+}availability [22]. Although, we did not measure Ca^{2+} homeostasis and signaling, a limitation in the current study, these studies in combination with the current study provide further evidence that the balance in mitochondrial dynamics is essential in maintaining skeletal muscle Ca^{2+} homeostasis and insulin sensitivity. Several studies recently reported that a Drp1 knockout in skeletal muscle induced muscle atrophy. In the present study, we also investigated the effect of the partial Drp1 knockout on skeletal muscle phenotype. We observed that the skeletal muscle Drp1 knockout did not alter muscle mass or muscle fiber size. This is consistent with a previous study utilizing a similar heterozygous skeletal muscle Drp1 knockout [21] but contradictory to three other studies [22–24]. These inconsistencies may be explained by the difference in the degree and duration to which skeletal muscle Drp1 was reduced. Specifically, Favaro and colleagues [22] utilized a homozygous skeletal muscle-

specific Drp1 ablation mouse model (>90% reduction of Drp1 content) and found significant skeletal muscle atrophy, whereas Moore and colleagues [21] and our study used heterozygous partial Drp1 knockout (i.e., ~30% Drp1 reduction) and found no detrimental effect on muscle mass and quality. However, detrimental effects on skeletal muscle quality may occur in our mDrp1$^{+/-}$ mice following long-term Drp1 inhibition. Dulac and colleagues [23,24] recently observed robust muscle atrophy and impaired muscle function at 4-months following the partial skeletal muscle Drp1 knockdown using an intramuscular adenine-associated virus (AAV) transfection. Collectively, potential therapies targeting Drp1 need further investigations to adjust its content in a specific range to improve insulin sensitivity without compromising muscle growth and function in long term.

Our study has some limitations. First, we focused on male mice to avoid hormone effects on mitochondrial fission and insulin sensitivity, as previous studies have demonstrated that Drp1 activity was heavily influenced by estrogen [21,64]. Second, *in vivo* mitochondrial function was assessed in isolated mitochondria, which may only isolate subsarcolemmal mitochondria and also cause damage during the isolation process [65]. The advantage of this approach is that it allows us to test mitochondrial function without the influence of the cytoskeleton and endoplasmic reticulum [66]. Regardless, future work should consider using permeabilized muscle fibers to mimic the physiological condition in skeletal muscle better, which may have different findings than the current study. Lastly, several mitochondrial assessments (e.g., respiration, complex activity) were performed only in one muscle type. A previous study has shown that mitochondrial quality control and function may be differentially affected by interventions in different muscle types [67]. Therefore, fiber type differences should be considered in future studies by assessing mitochondria in additional muscles (e.g., soleus and EDL).

5. CONCLUSION

In conclusion, our findings provide definitive evidence that partial loss of skeletal muscle Drp1 is sufficient in enhancing whole-body glucose homeostasis and insulin sensitivity in obesity-induced insulin-resistant conditions. In addition, our findings reveal divergent effects of Drp1 on whole-body metabolic phenotypes under lean healthy, and obese insulin-resistant conditions. These metabolic improvements induced by reducing Drp1 content in obese insulin-resistant conditions are partly due to reduced mitochondrial-derived H_2O_2 production, resulting from rebalanced mitochondrial dynamics and improved mitochondrial integrity. Collectively, these findings indicate that targeting skeletal muscle Drp1 may be a viable approach to counter obesity-induced insulin resistance.

DECLARATION OF COMPETING INTEREST

K.Z. receives grant funding from Remedium Bio, but not relevant to this article. No other potential conflicts of interest were reported.

DATA AVAILABILITY

Data will be made available on request.

ACKNOWLEDGMENTS

We want to take this opportunity to thank the Center for Personalized Cancer Therapy at UMass Boston for sharing their core equipment.

This study was supported by grants from the National Institutes of Health (R15DK131512, KZ), (R01AR050429, ZY) and (S10 OD025113-01, GMH), Diabetes Action Research and Education Foundation (KZ), UMass Boston Proposal Development Grant (KZ), UMass Boston Doctoral Dissertation Research Grant (BAK), Craig R. Bollinger Memorial Research Grant (BAK), and the Ronald E. McNair Post-Baccalaureate Achievement Program (PN).

APPENDIX A. SUPPLEMENTARY DATA

Supplementary data to this article can be found online at https://doi.org/10.1016/j.molmet.2023.101802.

REFERENCES

[1] DeFronzo RA, Tripathy D. Skeletal muscle insulin resistance is the primary defect in type 2 diabetes, Diabetes Care. American Diabetes Association; 2009. p. S157–63.
[2] Fisher-Wellman KH, Neufer PD. Linking mitochondrial bioenergetics to insulin resistance via redox biology. Trends Endocrinol Metabol 2012;23(3):142–53.
[3] Di Meo S, Iossa S, Venditti P. Skeletal muscle insulin resistance: role of mitochondria and other ROS sources. J Endocrinol 2017;233(1):R15–42.
[4] Liu R, Jin P, Yu L, Wang Y, Han L, Shi T, et al. Impaired mitochondrial dynamics and bioenergetics in diabetic skeletal muscle. PLoS ONE 2014;9(3):1–9.
[5] Archer SL. Mitochondrial dynamics - Mitochondrial fission and fusion in human diseases. N Engl J Med 2013;369(23):2236–51.
[6] Fealy CE, Mulya A, Axelrod CL, Kirwan JP. Mitochondrial dynamics in skeletal muscle insulin resistance and type 2 diabetes. Transl Res 2018;202:69–82.
[7] Hood DA, Memme JM, Oliveira AN, Triolo M. Maintenance of Skeletal Muscle Mitochondria in Health, Exercise, and Aging. Annu Rev Physiol 2019;81:19–41.
[8] Rambold AS, Kostelecky B, Elia N, Lippincott-Schwartz J. Tubular network formation protects mitochondria from autophagosomal degradation during nutrient starvation. PNAS 2011;108(25):10190–5.
[9] Gundersen AE, Kugler BA, McDonald PM, Veraksa A, Houmard JA, Zou K. Altered Mitochondrial Network Morphology and Regulatory Proteins in Mitochondrial Quality Control in Myotubes from Severely Obese Humans With or Without Type 2 Diabetes. Appl Physiol Nutr Metabol 2020;45(3):283–93.
[10] Kristensen MD, Petersen SM, Møller KE, Lund MT, Hansen M, Hansen CN, et al. Obesity leads to impairments in the morphology and organization of human skeletal muscle lipid droplets and mitochondrial networks, which are resolved with gastric bypass surgery-induced improvements in insulin sensitivity. Acta Physiol 2018;224(4):e13100.
[11] Giovarelli M, Zecchini S, Martini E, Garrè M, Barozzi S, Ripolone M, et al. Drp1 overexpression induces desmin disassembling and drives kinesin-1 activation promoting mitochondrial trafficking in skeletal muscle. Cell Death Differ 2020;27:2383–401.
[12] Touvier T, De Palma C, Rigamonti E, Scagliola A, Incerti E, Mazelin L, et al. Muscle-specific Drp1 overexpression impairs skeletal muscle growth via translational attenuation. Cell Death Dis 2015;6(2).
[13] Fealy CE, Mulya A, Lai N, Kirwan JP. Exercise training decreases activation of the mitochondrial fission protein dynamin-related protein-1 in insulin-resistant human skeletal muscle. J Appl Physiol 2014;117:239–45.
[14] Kugler BA, Gundersen AE, Li J, Deng W, Eugene N, Gona PN, et al. Roux-en-Y gastric bypass surgery restores insulin-mediated glucose partitioning and mitochondrial dynamics in primary myotubes from severely obese humans. Int J Obes 2020;44(3):684–96.
[15] Axelrod CL, Fealy CE, Erickson ML, Davuluri G, Fujioka H, Dantas WS, et al. Lipids activate skeletal muscle mitochondrial fission and quality control

networks to induce insulin resistance in humans. Metabolism: Clinical and Experimental; 2021.
[16] Kugler BA, Deng W, Francois B, Nasta M, Hinkley JM, Houmard JA, et al. Distinct Adaptations of Mitochondrial Dynamics to Electrical Pulse Stimulation in Lean and Severely Obese Primary Myotubes. Med Sci Sports Exerc 2020;53(6):1151–60.
[17] Jheng H-F, Tsai P-J, Guo S-M, Kuo L-H, Chang C-S, Su I-J, et al. Mitochondrial fission contributes to mitochondrial dysfunction and insulin resistance in skeletal muscle. Mol Cell Biol 2012;32(2):309–19.
[18] Kugler BA, Deng W, Duguay AL, Garcia JP, Anderson MC, Nguyen PD, et al. Pharmacological inhibition of dynamin-related protein 1 attenuates skeletal muscle insulin resistance in obesity. Physiol Rep 2021;9(7):e14808.
[19] Smith Melissa E, Tippetts Trevor S, Brassfield Eric S, Tucker Braden J, Ockey A, Swensen Adam C, et al. Mitochondrial fission mediates ceramide-induced metabolic disruption in skeletal muscle. Biochem J 2013;456(3): 427–39.
[20] Bordt EA, Clerc P, Roelofs BA, Sesaki H, Hill RB, Polster Correspondence BM. The Putative Drp1 Inhibitor mdivi-1 Is a Reversible Mitochondrial Complex I Inhibitor that Modulates Reactive Oxygen Species. Dev Cell 2017;40:583–94.
[21] Moore TM, Zhou Z, Cohn W, Norheim F, Lin AJ, Kalajian N, et al. The impact of exercise on mitochondrial dynamics and the role of Drp1 in exercise performance and training adaptations in skeletal muscle. Mol Metabol 2019;21:51–67.
[22] Favaro G, Romanello V, Varanita T, Andrea Desbats M, Morbidoni V, Tezze C, et al. DRP1-mediated mitochondrial shape controls calcium homeostasis and muscle mass. Nat Commun 2019;10:2576.
[23] Dulac M, Leduc-Gaudet JP, Cefis M, Ayoub MB, Reynaud O, Shams A, et al. Regulation of muscle and mitochondrial health by the mitochondrial fission protein Drp1 in aged mice. J Physiol 2021;599(17):4045–63.
[24] Dulac M, Leduc-Gaudet JP, Reynaud O, Ayoub MB, Guérin A, Finkelchtein M, et al. Drp1 knockdown induces severe muscle atrophy and remodelling, mitochondrial dysfunction, autophagy impairment and denervation. J Physiol 2020;0:1–20.
[25] Wakabayashi J, Zhang Z, Wakabayashi N, Tamura Y, Fukaya M, Kensler TW, et al. The dynamin-related GTPase Drp1 is required for embryonic and brain development in mice. J Cell Biol 2009;186(6):805–16.
[26] Benedé-Ubieto R, Estévez-Vázquez O, Ramadori P, Cubero FJ, Nevzorova YA. Guidelines and Considerations for Metabolic Tolerance Tests in Mice. Diabetes, Metab Syndrome Obes Targets Ther 2020;13:439.
[27] Nagy C, Einwallner E. Study of In Vivo Glucose Metabolism in High-fat Diet-fed Mice Using Oral Glucose Tolerance Test (OGTT) and Insulin Tolerance Test (ITT). J Vis Exp: JoVE 2018;2018(131):56672.
[28] Virtue S, Vidal-Puig A. GTTs and ITTs in mice: simple tests, complex answers. Nat Metabol 2021;3(7):883–6.
[29] Tarnopolsky MA, Rennie CD, Robertshaw HA, Fedak-Tarnopolsky SN, Devries MC, Hamadeh MJ. Influence of endurance exercise training and sex on intramyocellular lipid and mitochondrial ultrastructure, substrate use, and mitochondrial enzyme activity. Am J Physiol Regul Integr Comp Physiol 2007;292(3):R1271–8.
[30] Wen Y, Murach KA, Vechetti Jr IJ, Fry CS, Vickery C, Peterson CA, et al. MyoVision: software for automated high-content analysis of skeletal muscle immunohistochemistry. J Appl Physiol 2018;124(1):40–51. 1985.
[31] Thome T, Salyers ZR, Kumar RA, Hahn D, Berru FN, Ferreira LF, et al. Uremic metabolites impair skeletal muscle mitochondrial energetics through disruption of the electron transport system and matrix dehydrogenase activity. Am J Physiol Cell Physiol 2019;317:C701–13.
[32] Quinlan CL, Orr AL, Perevoshchikova IV, Treberg JR, Ackrell BA, Brand MD. Mitochondrial Complex II Can Generate Reactive Oxygen Species at High Rates in Both the Forward and Reverse Reactions. J Biol Chem 2012;287(32): 27255–64.
[33] Wong H-s, Monternier P-a, Orr AL, Brand MD. Plate-Based Measurement of Superoxide and Hydrogen Peroxide Production by Isolated Mitochondria. Mitochondrial Bioenergetics: Methods and Protocols 2018;1782:287–99.
[34] Hinkley JM, Zou K, Park S, Zheng D, Dohm GL, Houmard JA. Differential acute and chronic responses in insulin action in cultured myotubes following from nondiabetic severely obese humans following gastric bypass surgery. Surg Obes Relat Dis 2017;13(11):1853–62.
[35] Valente AJ, Maddalena LA, Robb EL, Moradi F, Stuart JA. A simple ImageJ macro tool for analyzing mitochondrial network morphology in mammalian cell culture. Acta Histochem 2017;119(3):315–26.
[36] Severinsen MCK, Pedersen BK. Muscle-Organ Crosstalk: The Emerging Roles of Myokines. Endocr Rev 2020;41(4):594–609.
[37] Coskun T, Bina HA, Schneider MA, Dunbar JD, Hu CC, Chen Y, et al. Fibroblast Growth Factor 21 Corrects Obesity in Mice. Endocrinology 2008;149(12): 6018–27.
[38] Kharitonenkov A, Shiyanova TL, Koester A, Ford AM, Micanovic R, Galbreath EJ, et al. FGF-21 as a novel metabolic regulator. J Clin Invest 2005;115(6):1627–35.
[39] Bach D, Naon D, Pich S, Soriano FX, Vega N, Rieusset J, et al. Expression of Mfn2, the Charcot-Marie-Tooth Neuropathy Type 2A Gene, in Human Skeletal Muscle. Diabetes 2005;54:2685–93.
[40] Bach D, Pich S, Soriano FX, Vega N, Baumgartner B, Oriola J, et al. Mitofusin-2 Determines Mitochondrial Network Architecture and Mitochondrial Metabolism. J Biol Chem 2003;278(19):17190–7.
[41] Leduc-Gaudet JP, Reynaud O, Chabot F, Mercier J, Andrich DE, St-Pierre DH, et al. The impact of a short-term high-fat diet on mitochondrial respiration, reactive oxygen species production, and dynamics in oxidative and glycolytic skeletal muscles of young rats. Physiol Rep 2018;6(4):e13548.
[42] Losón OC, Song Z, Chen H, Chan DC. Fis1, Mff, MiD49, and MiD51 mediate Drp1 recruitment in mitochondrial fission. MBoC 2013;24:659–67.
[43] Otera H, Wang C, Cleland MM, Setoguchi K, Yokota S, Youle RJ, et al. Mff is an essential factor for mitochondrial recruitment of Drp1 during mitochondrial fission in mammalian cells. J Cell Biol 2010;191(6):1141.
[44] Ortenblad N, Mogensen M, Petersen I, Hojlund K, Levin K, Sahlin K, et al. Reduced insulin-mediated citrate synthase activity in cultured skeletal muscle cells from patients with type 2 diabetes: evidence for an intrinsic oxidative enzyme defect. Biochim Biophys Acta 2005;1741(1-2):206–14.
[45] Boyle KE, Zheng D, Anderson EJ, Neufer PD, Houmard JA. Mitochondrial lipid oxidation is impaired in cultured myotubes from obese humans. Int J Obes (Lond) 2012;36(8):1025–31.
[46] Hoeks J, Wilde J, Hulshof MF, Berg SA, Schaart G, Dijk KW, et al. High fat diet-induced changes in mouse muscle mitochondrial phospholipids do not impair mitochondrial respiration despite insulin resistance. PLoS One 2011;6(11): e27274.
[47] Ferrara PJ, Lang MJ, Johnson JM, Watanabe S, McLaughlin KL, Maschek JA, et al. Weight loss increases skeletal muscle mitochondrial energy efficiency in obese mice. Life Metab 2023;2(2).
[48] Naples SP, Borengasser SJ, Rector RS, Uptergrove GM, Morris EM, Mikus CR, et al. Skeletal muscle mitochondrial and metabolic responses to a high-fat diet in female rats bred for high and low aerobic capacity. Appl Physiol Nutr Metab 2010;35(2):151–62.
[49] Lee H, Ha TY, Jung CH, Nirmala FS, Park SY, Huh YH, et al. Mitochondrial dysfunction in skeletal muscle contributes to the development of acute insulin resistance in mice. J Cachexia Sarcopenia Muscle 2021;12(6):1925–39.
[50] Powers SK, Ji LL, Kavazis AN, Jackson MJ. Reactive oxygen species: Impact on skeletal muscle. Compr Physiol 2011;1(2):941–69.
[51] Lin H-Y, Weng S-W, Chang Y-H, Su Y-J, Chang C-M, Tsai C-J, et al. The Causal Role of Mitochondrial Dynamics in Regulating Insulin Resistance in Diabetes: Link through Mitochondrial Reactive Oxygen Species. Hindawi Oxidative Medicine and Cellular Longevity 2018:14. 2018.

[52] Anderson EJ, Lustig ME, Boyle KE, Woodlief T, Kane DA, Lin C-T, et al. Mitochondrial H2O2 emission and cellular redox state link excess fat intake to insulin resistance in both rodents and humans. J Clin Invest 2009;119(3):573–81.

[53] Fisher-Wellman KH, Gilliam LAA, Lin CT, Cathey BL, Lark DS, Darrell Neufer P. Mitochondrial glutathione depletion reveals a novel role for the pyruvate dehydrogenase complex as a key H2O2 emitting source under conditions of nutrient overload. Free Radic Biol Med 2013;65:1201.

[54] Lefort N, Glancy B, Bowen B, Willis WT, Bailowitz Z, De Filippis EA, et al. Increased reactive oxygen species production and lower abundance of complex I subunits and carnitine palmitoyltransferase 1B protein despite normal mitochondrial respiration in insulin-resistant human skeletal muscle. Diabetes 2010;59(10):2444–52.

[55] Quinlan CL, Perevoshchikova IV, Hey-Mogensen M, Orr AL, Brand MD. Sites of reactive oxygen species generation by mitochondria oxidizing different substrates. Redox Biol 2013;1(1):304–12.

[56] He J, Watkins S, Kelley DE. Skeletal Muscle Lipid Content and Oxidative Enzyme Activity in Relation to Muscle Fiber Type in Type 2 Diabetes and Obesity. Diabetes 2001;50:817–23.

[57] Ngo DTM, Sverdlov AL, Karki S, Macartney-Coxson D, Stubbs RS, Farb MG, et al. Mitochondria Dysfunction in Aging and Metabolic Diseases: Oxidative modifications of mitochondrial complex II are associated with insulin resistance of visceral fat in obesity. Am J Physiol Endocrinol Metabol 2019;316(2):E168.

[58] Oberbach A, Bossenz Y, Lehmann S, Niebauer J, Adams V, Paschke R, et al. Altered Fiber Distribution and Fiber-Specific Glycolytic and Oxidative Enzyme Activity in Skeletal Muscle of Patients With Type 2 Diabetes. Diabetes Care 2006;29(4):895–900.

[59] Mensink M, Hesselink MKC, Russell AP, Schaart G, Sels JP, Schrauwen P. Improved skeletal muscle oxidative enzyme activity and restoration of PGC-1α and PPARβ/δ gene expression upon rosiglitazone treatment in obese patients with type 2 diabetes mellitus. Int J Obes 2007;31(8):1302–10.

[60] Bonnard C, Durand A, Peyrol S, Chanseaume E, Chauvin M-A, Morlo B, et al. Mitochondrial dysfunction results from oxidative stress in skeletal muscle of diet-induced insulin-resistant mice. J Clin Invest 2008;118(2):789–800.

[61] Holmstrom MH, Iglesias-Gutierrez E, Zierath JR, Garcia-Roves PM. Tissue-specific control of mitochondrial respiration in obesity-related insulin resistance and diabetes. AJP: Endocrinol Metabol 2012;302(6):E731–9.

[62] Samocha-Bonet D, Campbell LV, Mori TA, Croft KD, Greenfield JR, Turner N, et al. Overfeeding Reduces Insulin Sensitivity and Increases Oxidative Stress, without Altering Markers of Mitochondrial Content and Function in Humans. PLoS ONE 2012;7(5):e36320.

[63] Paul Dhiraj, Aichler M, Sonja Pfuhlmann K, Verónica, et al. Calcineurin Links Mitochondrial Elongation with Energy Metabolism. Cell Metabol 2015;22(5):838–50.

[64] Ribas V, Drew BG, Zhou Z, Phun J, Kalajian NY, Soleymani T, et al. Skeletal muscle action of estrogen receptor a is critical for the maintenance of mitochondrial function and metabolic homeostasis in females. Sci Transl Med 2016;8:334ra354.

[65] Lanza IR, Nair KS. Functional Assessment of Isolated Mitochondria In Vitro. Methods Enzymol 2009;457:349–72.

[66] Lai N, Kummitha CM, Rosca MG, Fujioka H, Tandler B, Hoppel CL. Isolation of mitochondrial subpopulations from skeletal muscle: optimizing recovery and preserving integrity. Acta Physiol (Oxford, England) 2019;225(2):e13182.

[67] Leduc-Gaudet JP, Reynaud O, Chabot F, Mercier J, Andrich DE, St-Pierre DH, et al. The impact of a short-term high-fat diet on mitochondrial respiration, reactive oxygen species production, and dynamics in oxidative and glycolytic skeletal muscles of young rats. Physiol Rep 2018;6(4).

